Chapter 2

OVERVIEW OF THE PROPOSED STUDY

This chapter gives an overview of the proposed study. To define the illicit material detection problem, in Section 2.1, the types of illicit materials are first introduced. The environment in which these illicit materials need to be detected is also carefully described. In Section 2.2, x-ray physics is discussed in detail. In Section 2.3, the principle of illicit material detection using x-ray technologies is discussed. A review is then given to different types of x-ray technologies that can be used for illicit material detection. This occurs in Section 2.4. X-ray technologies provide the ability to determine an object's *density* and Z_{eff} information. Knowing those two pieces of information about an object, its material type can theoretically be uniquely determined. Section 2.5 discusses the sensing technologies and other related problems needed to derive these two pieces of information. In order to derive R, a Z_{eff}-related information, and L, a *density*-related information, an object's *true* gray levels must be determined. Section 2.6 sets the research goal for this dissertation, which is to develop an advanced image-processing system in order to reveal an object's *true* gray levels. Section 2.7 describes the hardware of the multiple sensor system that was used to collect x-ray images used in this study. Finally, Section 2.8 summaries the important points that are presented.

2.1 Illicit Materials and Illicit Material Detection

Illicit materials are materials that either may present a danger to the public or are unlawfully possessed by an individual. There are basically two categories of illicit

materials: explosives and drugs. In this dissertation, the focus is on the detection of explosive materials.

Modern industry has developed explosives not only for military purposes, but also for civilian uses, such as construction and mining. Explosives, especially military explosives, such as C4 and Semtex, are very powerful. In the past several years, state-sponsored terrorists have been able to smuggle high power explosives into civilian aircraft by hiding them inside luggage bags. Those explosives are usually detonated in mid-air and basically destroy an aircraft. Killing all or most of the people aboard. One vivid memory for everyone is the bombing of Pan Am-103 in 1988 over Scotland. The danger present to the public, and the political impact of such terrorists' acts, cannot be underestimated. Besides the bombing of aircraft, another type of powerful terrorists' act is truck bombing. The victims from this type of bombing actually exceed the victims from the bombing of aircraft. There is only one purpose for such terrorists' bombing: to terrorize a nation. Their acts have presented great danger to civilians. This forces the Federal Government to adopt systematic means by which to guard the national security. A search for a technical solution to this problem has intensified.

Compared to explosives, drug interdiction attracts less public concern because it does not present the same danger to the public. Drugs are usually carried by traffickers who attempt to disguise their presence. For example, when transported by a truck, drugs are often placed inside the tires, inside the driver's seats, or disguised as other commerce. Again, a technical solution to finding drugs would be helpful for intercepting drugs.

Table 2.1-1 [GOZ91] shows a list of 50 commonly seen materials in the detection environment. Those materials are categorized into three groups: explosives, innocuous common materials, and drugs. Among all the explosives, the most dangerous to the public are plastic explosives [NOV94]. Plastic explosives, such as Semtex, are odorless and malleable, and they are easy to conceal. They pose serious problems for detection because they cannot be found based on their shape or metal components. The only way

to detect them is to measure an object's physical or chemical properties, and use those properties to infer an object's material type.

Table 2.1-1 Explosives, drugs, and various common materials

Innocuous Materials	Explosives	Drugs
Wool	Nitroglycerin	heroin
Silk	EDGN	HHCL
dacron	amnit	cocaine
orlon	black powder	COCL
nylon	ncel	morph
cotton	PETN	PCP
rayon	detasheet	LSD
polyethylene	TNT	
polypropylene	comp-B	
PVC	PBSTY	
saran	tetryl	
lucite	DYN	
neoprene	HMX	
paper	C3	
alcohol	C4	
sugar	picric acid	
oil	triacetate	
barley	hexachloroethane	
soybean		
wood		
water		
polyurethane		
melamine		

There are two major categories of technologies that can be used for illicit material detection: vapor detection technology and bulk detection technology [NOV91]. Vapor detection technology uses a vapor detector to sense molecules vaporized from illicit materials [FIN91]. It is often used to detect quantities of airborne particles of illicit materials. It is not effective for detecting explosives that are packaged in plastic bags, metal cans, etc., because the vaporized molecules are confined to the space inside the bag or can, and cannot be sensed by the detector that is outside the bag or can. Thus, this technology is not considered as a very effective technology for detecting explosive materials in bags.

Bulk technology uses a source to generate a penetrating radiation and attempts to sense the interactions between this radiation and hidden explosives. Compared to vapor technology, bulk technology can easily detect illicit material types even when those materials are packaged in bags or cans. It has high sensitivity, selectivity, and penetration range. Comparing to vapor technology, bulk technology is more effective for detecting explosive materials in bags. There are a number of types of bulk technologies. Those are nuclear detection technologies, electromagnetic detection technologies, and x-ray detection technologies [NOV91]. The nuclear detection technology uses neutrons or gamma rays to react with different elemental components in the object of interest to produce a reaction particular to the specific detector application. The types of detection methods in this technology category include thermal neutron analysis, fast neutron analysis, pulsed fast neutron analysis, and resonance absorption [GRO91]. These technologies have the ability to penetrate large, thick, and dense materials, and are able to identify some of the chemical elements of particular interest [GOZ91]. However, the devices are expensive because it requires highly sophisticated techniques to build the radiation source and highly trained operators to operate the systems. The size of the equipment is usually very large [GOZ91]. Thus, the nuclear detection technology has not been put into practical use for detecting illicit materials.

There are many types of detection methods using electromagnetic detection technologies: nuclear magnetic resonance, nuclear quadrupole resonance, millimeter wave detection, and dielectric detection [NOV91]. Both the nuclear magnetic and quadrupole resonance

methods are to detect the effects of atoms and molecules based on radio frequency responses. Each atom or molecule has its own unique electromagnetic properties that responds to magnetic and radio frequency fields. Their difference is that the first method requires a magnetic field to be present while the radio frequency is pulsed through the object of interest; the second method does not need such a magnetic field. The nuclear quadrupole technology can be made inexpensive and portable. Though the nuclear quadrupole resonance technology is still years away from being put into practical use, it has been and continues to be a major research topic in the past several years. The millimeter wave detection method scans a holograph of an inspected object and detects the anomalies in this holograph. This method is only effective for detecting some explosives. The dielectric detection method detects bottle contents by measuring the dielectric constant of liquid. This method is still in the early stages of development and needs further development.

X-ray technologies are by far the most promising technology used for detecting explosive materials [CON93]. It provides a safe, inexpensive, yet relatively precise method for detecting illicit materials. It has been chosen as the technology used for this study. The remainder of this chapter discusses the theory and implementation of illicit material detection using x-ray technology.

2.2 X-ray Physics

2.2.1 X-ray source

X-rays are a form of electromagnetic wave with a wavelength range from 0.001 nm to 10 nm, or from 120 eV to 1.2 MeV in terms of the photon energies. Higher energy (shorter wavelength) photons are called γ-rays. An X-ray beam is generated when a stream of cathode-ray electrons is accelerated through a vacuum and strikes a metallic target. The soft x-rays used to inspect illicit materials usually have typical field potentials between 60 to 120 keV. The cathode typically employs a heated tungsten filament is the source of the electrons, and the target material used depends on the application. Figure 2.2-1 shows a schematic of this type of x-ray tube [DYS90].

When a high-energy electron beam bombards a solid target (anode), two processes happen: the Bremsstrahlung effect and line spectra. The Bremsstrahlung process is due to the deceleration of the incident electrons by coulomb interactions with the electrons and nuclei of the target material. The process gives a continuous spectrum. A line spectrum is caused by the removal of an inner-level atomic electron followed by relaxation of the atom with the emission of an x-ray beam [CHE96]. The line spectrum that occurs depends on the target material used. Figure 2.2-2 shows a continuous spectrum and a line spectrum of an x-ray tube [CHE97]. For this tube, the electron energy used is 150 keV, and the x-ray photons produced have a continuous spectrum between 0 keV up to 145 keV. The line spectrum shows up at around 70 keV. This particular line spectrum is a K spectrum; it is caused by the electron transitions that ultimately fill a vacancy in the K shell [CHE97].

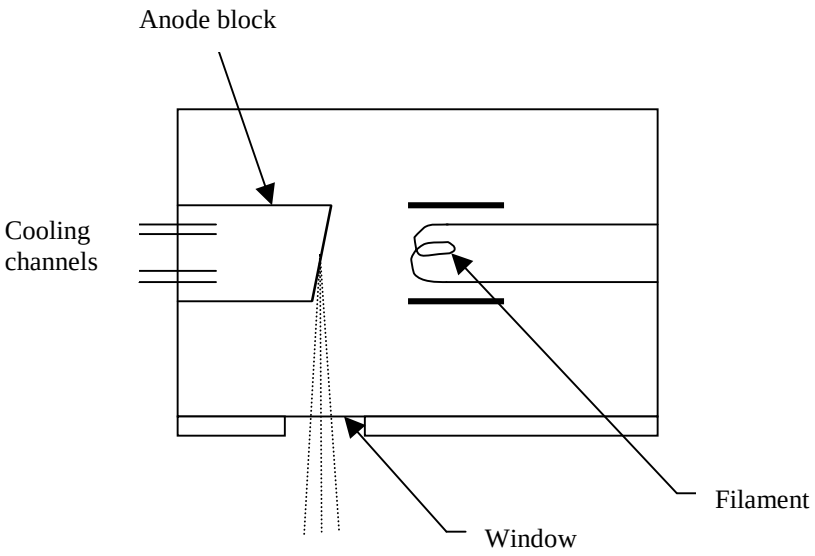

Figure 2.2-1 Conventional x-ray tube (schematic) [DYS90].

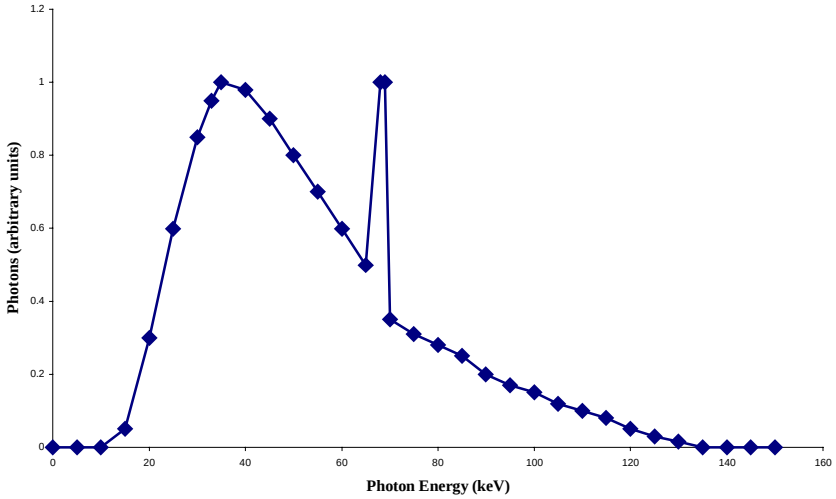

Figure 2.2-2 Continuous and line spectrum produced by an x-ray tube [CHE97].

Sometimes, a monochromatic x-ray source is desired for a system because in theory, the measured characteristic values of a material can be more precisely determined when this type of source is used [ZOU98]. A monochromatic x-ray beam is obtained either from a beam of polychromatic, "white" x-rays, or from a beam comprised of one or more characteristic x-ray emission lines superimposed on a white radiation background [DYS90]. In either case, monochromatization may result in either partial or total monochromatic x-rays. Partial monochromatization is cheaper and simpler to produce, and the loss of intensity is less than when total monochromatization is employed. However, no matter what kind of monochromatic source is used, the loss of energy is significant. Less energy of an x-ray beam means less penetration capability. Without strong penetration capability, the detection results may not be very precise. This explains why no commercial x-ray systems use a monochromatic source for detecting illicit materials.

2.2.2 X-ray interaction with matter

X-ray photons can penetrate solid materials that are opaque to lower-energy radiation [DYS90]. The interaction between x-ray electromagnetic radiation and matter represents one of the most varied classes of phenomena in the whole of experimental study. For now, I am only concerned with situations in which the overall behavior of an absorber or scatterer can be deduced by regarding it as a collection of individual atoms, each absorbing or scattering independently of its surroundings. In such cases one can assert that interactions between x-ray photons and matter are single, identifiable processes, each associated with an individual atom, and can therefore be characterized by a *cross-section* [DYS90].

The first phenomenon to study is x-ray transmission [DYS90]. When a beam of incident x-rays traverses through any material, its intensity is reduced. Suppose the incident radiation has an intensity of I, and is reduced by an amount δI on passing through a thin homogeneous layer of thickness δx, consisting of only one kind of atom. This is shown in Figure 2.2-3. Then the following equation is true [DYS90]:

$$-\frac{\delta I}{I} = \sigma n \delta x \tag{2.2-1}$$

where n is the number of atoms per unit volume and σ is the cross-section per atom. After integration, and assuming an incident intensity I_0, the following equation is obtained

$$I = I_0 e^{-\sigma n x} \tag{2.2-2}$$

For a compound material, the cross-section of a molecule is

$$\sigma = \sum_i \sigma_i \tag{2.2-3}$$

where i is the i^{th} element appearing in this compound. The cross-sections for elements were obtained from experiments performed by physicists during the past fifty years. The compilation of the cross sections can be found in [MCM69]. It should be noted that σ is not a constant for an atom; it varies depending on x-ray photon energies.

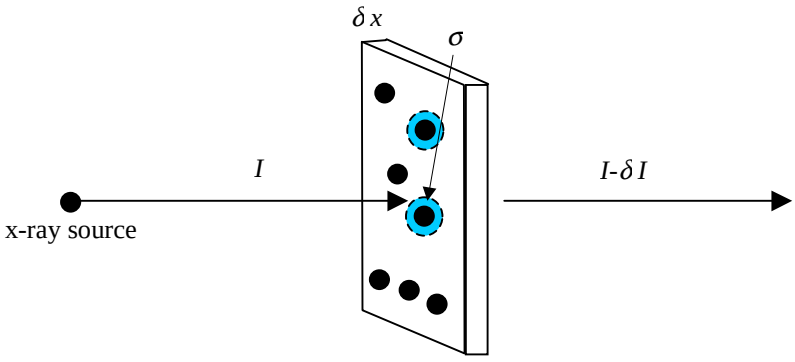

Figure 2.2-3 An illustration of x-ray transmission phenomenon.

There are three major processes of attenuation when a soft x-ray beam interacts with matter [MIC93]: (1) photoelectric effect; (2) coherent scattering; and (3) non-coherent scattering. The cross-section at an energy level can be separated into three 'partial' cross-sections σ_{pe}, σ_{cs}, and σ_{is} that correspond to the proportions of photoelectric absorption, coherent scatter, and incoherent scatter respectively. Thus

$$\sigma = \sigma_{pe} + \sigma_{cs} + \sigma_{is}. \tag{2.2-4}$$

The quantity σn is known as the total *linear attenuation coefficient* μ, and may also be written as [DYS90]

$$\mu = \frac{\sigma N \rho}{A} \tag{2.2-5}$$

where N is Avogadro's number, A is atomic weight, and ρ is the density of the matter. It is known that μ depends on the states (gas, liquid, or solid) of the absorbing material as well as on its nature (e.g. density), but μ/ρ is a constant for any substance regardless of its state. So μ/ρ is called the *mass absorption coefficient*, which is a characteristic value for a substance.

The photoelectric effect is one of the most important interactions in the soft x-ray energy region, a region that is between 1 and 100 keV [MIC93]. This effect is caused when an atom absorbs a photon and ejects an electron, as seen in Figure 2.2-4. In general, the inner electrons in the K, L, M shells are the predominating contributors to the photoelectric interaction. This effect occurs most readily if the binding energy is comparable with the photon energy, and has certain qualities of a resonance process.

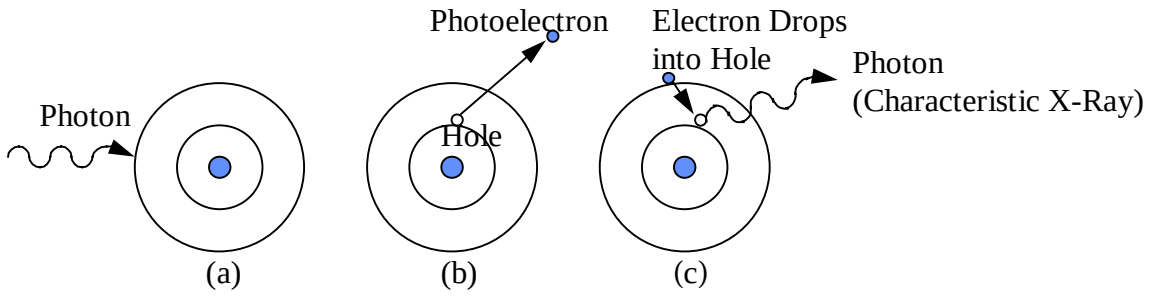

Figure 2.2-4 Photoelectric interaction with true absorption. (a) An incident photon loses all its energy on entering an atom, being absorbed in the process. (b) The atom responds by ejecting an inner shell electron, which becomes a photoelectron. The atom is now in an excited state. (c) An electron from a higher energy level fills the vacancy in the K-shell or L-shell, and emits a characteristic x-ray photon.

The photoelectric cross-section is determined by the nature of the absorber and the x-ray photon energy [MIC93]. It is found that σ_{pe} increases as Z or Z_{eff} of a material increases, where Z is the *atomic number* of a single element and Z_{eff} is the *effective atomic number* for a compound material. σ_{pe} also increases as the wavelength of x-ray increases. So I have

$$\sigma_{pe} \propto Z^n, \lambda^m \tag{2.2-6}$$

where n and m are two constants. The equation can be more precise if we know that the photon energy is far greater than the binding energy. In this case, n is known to be 5, and m is known to be *7/2*. The energy range we are using falls into this case, so in most of my studies, σ_{pe} could be expressed as

$$\sigma_{pe} \propto Z^5, \lambda^{7/2} \tag{2.2-7}$$

Coherent scattering occurs when an incident photon interacts with an electron, but has insufficient energy to overcome its binding energy. The photon is thus “scattered”, or

deflected from its original path, without energy loss. Figure 2.2-5 illustrates this situation.

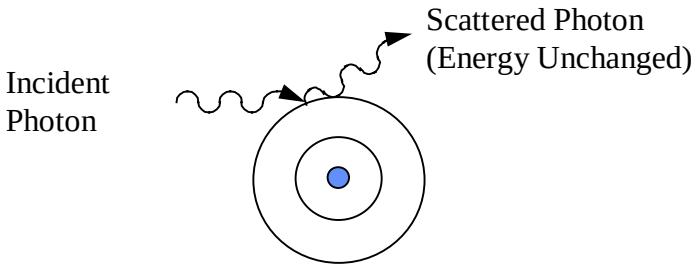

Figure 2.2-5 Coherent scattering. The incident x-ray photon is deflected from its original path without energy loss.

Coherent scattering can be considered as a free electron scattering of unpolarized radiation, plus the cooperative effect of all the electrons in an atom. For an x-ray wavelength larger than the diameter of the scattering atoms, the atomic cross section for coherent scattering is given by [DYS90]

$$\sigma_{cs} = 4\pi\left(\frac{e^2}{mc^2}\right)Z^2\left(\frac{\lambda}{2\pi a_T}\right)^2\left(0.8-\frac{\lambda}{8a_T}\right) \qquad (2.2\text{-}8)$$

where $a_T = 0.885Z^{-1/3}$ is the effective atomic radius.

The Compton effect, or incoherent scattering, is the process in which a photon interacts with a loosely bound or "free" electron as seen in Figure 2.2-6 [DYS90]. The result of this process is a photon with reduced energy being produced and deflected from the original direction. A Compton electron is also produced in some cases.

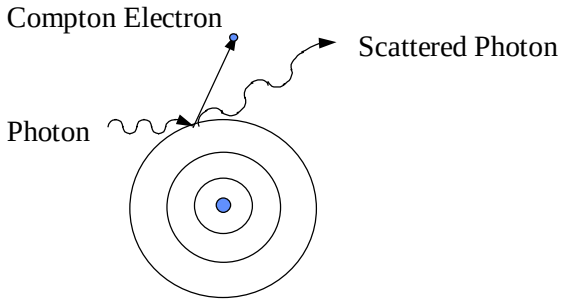

Figure 2.2-6 Compton interaction and scattering. Part of the photon's energy has been used up in removing a loosely bound orbital electron. Therefore, the emerging photon has less energy, and it has also undergone a change in direction [DYS90].

The cross-section of Compton scattering is given by

$$\sigma_{is}(\lambda_0) = \pi r_0^2 \lambda_0 \left\{ [1 - 2\lambda_0(\lambda_0 + 1)] \ln \frac{\lambda_0 + 2}{\lambda_0} + 4\lambda_0 + 2\frac{1 + \lambda_0}{(2 + \lambda_0)^2} \right\} \tag{2.2-9}$$

The relative strengths, in terms of a linear attenuation coefficient μ, for these processes are plotted as functions of photon energies in Figure 2.2-7 [MIC93]. It can be seen that for x-rays with energy less than about 2 keV, incoherent scattering is negligible and that coherent scattering accounts for less than 1% of the interaction. The dominant process is photoelectric absorption. For higher energies, scattering becomes more important, primarily because the absorption cross-section decrease more rapidly than the scattering cross-sections with increasing energy.

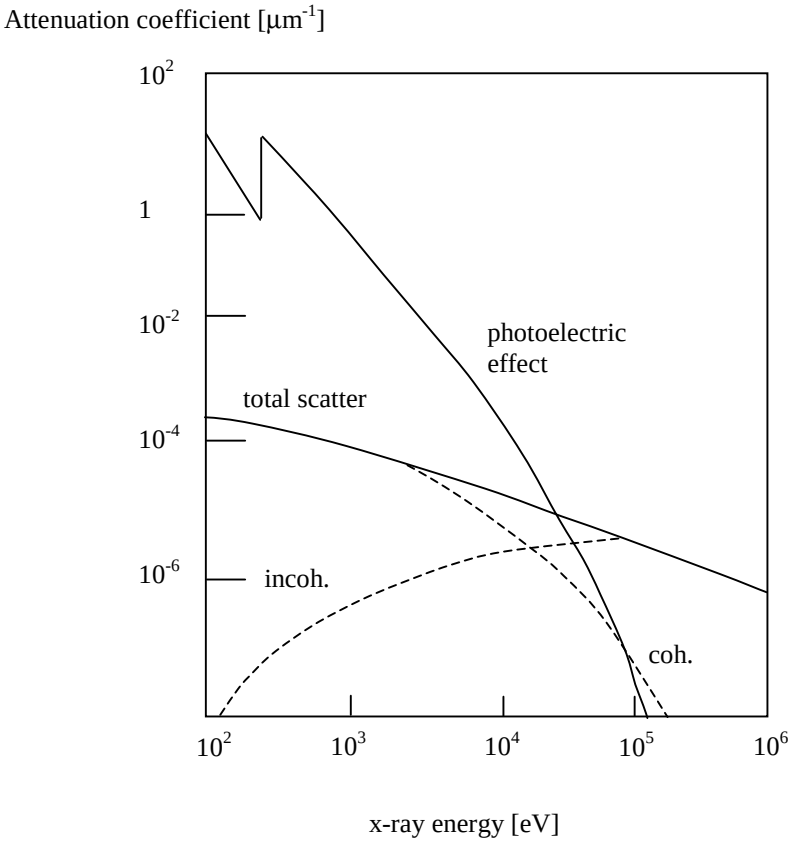

Figure 2.2-7 The strength of X-ray scattering and photoelectric effects.

The energy absorbed by the photoelectric effect or scattered by coherent and incoherent scattering can be computed as follows [MIC93]:

$$I_{pe} = I_0\left(1 - e^{-\sigma nx}\right)\frac{\sigma_{pe}}{\sigma} \tag{2.2-10}$$

$$I_{cs} = I_0\left(1 - e^{-\sigma nx}\right)\frac{\sigma_{cs}}{\sigma} \tag{2.2-11}$$

$$I_{is} = I_0\left(1 - e^{-\sigma nx}\right)\frac{\sigma_{is}}{\sigma} \tag{2.2-12}$$

In addition to the scattering, two new concepts are introduced here: forward scattering and backscattering. The illustration is given in Figure 2.2-8. θ is the angle between the

direction of the incident x-ray beam and the traveling direction of the photon that is being scattered or transmitted. The transmission of an x-ray beam refers to the x-ray photons with θ equal to 0°. Forward scattering refers to the scattered x-ray photons with θ that are less than 90° but greater than 0°. Backscattering refers to the scattered photons with θ that are greater than 90°. For most x-ray detection systems, a detector can be only placed either side by side or face to face with a x-ray source. If the detector is placed on the same side with the x-ray source, the signal detected is the backscatter signal. If the detector is placed on the opposite side of the scanning tunnel and the inspecting object is inserted between the source and detector, the signal detected is the forward scatter signal.

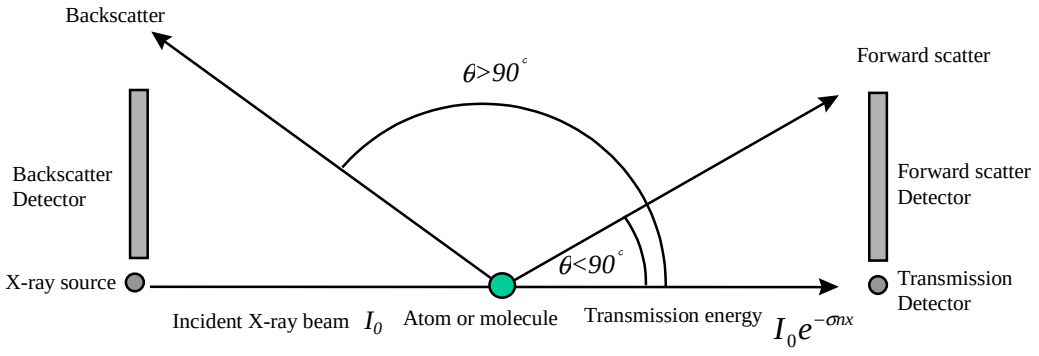

Figure 2.2-8 Illustration of forward scatter, backscatter, and transmission signals.

Though forward scatter and backscatter energy are proportional to the total scatter energy; there is no closed-form equation that describes the relationship between the partial scatter and the total scatter that can be used for real-time computation. The distribution probability of the scattered photons, the detector geometry, and the distance between an inspected object and the detector are factors affecting the strength of the forward or backward scattered signals. Most of those factors are unknown. Thus, using the forward or backward scattering signal, the total scattering energy cannot be easily computed.

2.2.3 X-ray detector

The operation of a scintillation detector depends on the luminescence of a crystal when excited by ionizing radiation. Photons are produced in the visible region and then are allowed to impinge on a photodiode. The photodiode converts the energy of visible photons to an electrical current, which is then sensed electronically [TAK90].

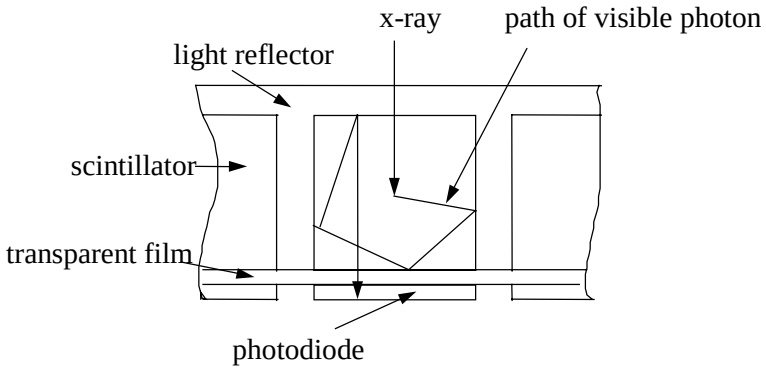

Figure 2.2-9 Schematic illustration of the structure of an x-ray detector. An x-ray photon is converted to visible photons which are detected by a photodiode after several reflections on surfaces of the scintillator [TAK90].

Scintillators are usually classified as organic or inorganic. Inorganic scintillators are preferred for x-ray studies because of their high level of photoelectric absorption. The structure of a scintillation detector is shown in Figure 2.2-9 [TAK90]. X-rays enter a scintillator material and produce visible photons by luminescence. These visible photons pass through a film and are detected by a photodiode. The mirror-polish scintillator is normally surrounded by an optical light reflector to ensure maximum channeling of light to the photodiode. One face of the scintillator is covered with a transparent film that is in contact with the photodiode. This film smoothes any remaining craters on the polished surface and ensures maximum transmission of light into the photodiode.

2.3 Principles of X-ray Detection

The *density* of a material is a measure of how much mass is contained in 1 cubic centimeter of that material. The *atomic number Z* of an element is equal to the number of protons in the atomic nucleus [DYS90]. The *effective atomic number* Z_{eff} of a compound is related to the atomic numbers of the elements in the compound and non-linearly to their respective proportions. There are a number of ways to compute *effective atomic number* [ZOU98]. A simple and commonly used method involves first computing the mass electron density $N_{g,i}$ of the i^{th} element using

$$N_{g,i} = \frac{N_A \omega_i Z_i}{M_i}. \tag{2.3-1}$$

The effective mass electron density of the compound molecule N_g is then computed using

$$N_g = \sum_i N_{g,i}. \tag{2.3-2}$$

The fractional number α_i of electrons is then computed from

$$\alpha_i = \frac{N_{g,i}}{N_g}. \tag{2.3-3}$$

The Z_{eff} of the compound molecule is finally computed based on

$$Z_{eff} = \left(\sum_i \alpha_i Z_i^{m-1} \right)^{1/(m-1)} \tag{2.3-4}$$

where m is a constant between 3.0 to 5.0, which of these values that is used depends on the material's composition and the photon energy. It is suggested that m is set to 4.1 for a material with Z_{eff} higher than 6, and 3.6 for materials with Z_{eff} less than 6 [ZOU98].

When common substances found in luggage are plotted on a chart that maps Z_{eff} vs. *density* along with various threat materials as seen in Figure 2.3-1 [EIL92], a pattern emerges that suggests a way to distinguish plastic explosives and drugs from the vast majority of commonly seen innocuous materials. Plastic explosives, including Semtex, C4, Detasheet, PE-4, and other explosives with an RDX or PETN base, fall within a relatively narrow window in Z_{eff} and in *density*. Those explosives are considered to be the highest threat because of their large explosive power per unit mass, their capability of being molded into almost any shape, and their ready availability to terrorists. Other explosives such as TNT and ammonium-nitrate based explosives also tend to fall within the same Z_{eff} window at differing densities. Heroin and cocaine hydrochlorides are grouped together with similar densities and Z_{eff} values. Their Z_{eff} is somewhat higher than typical innocuous materials.

The basic elemental signatures define only a theoretical discrimination capability between illicit materials and innocuous materials. It assumes a perfect measurement and observation of the pure (unmixed) illicit or innocuous material. In reality, the measurements are far from perfect and observations are made over volumes larger than the ones occupied by the pure materials [GRO91]. X-ray technologies are sensitive to the overall *density* and Z_{eff} of the constituents. The physical principles of x-ray interactions can be used to interpret the results to deduce the types of material present in the detection environment [SCH91]. Note that in Figure 2.3-1 chocolate, honey, and other things that can be confused with explosives are not shown, because these substances are not used by the FAA to test a system's detection capability. However, those materials have very similar *density* and Z_{eff} as explosive materials, and may be easily put into the cluster of explosives. So one should notice that even in this ideal *density*-Z_{eff} detection chart the discrimination of explosives is not perfect.

Density and Z_{eff} are not the only characteristic values that x-ray technologies can provide for a material. There are other values such as the scatter spectra can also be used for determining an object's material type. However *density* and Z_{eff} are chosen because they

are the easiest to determine based on x-ray based measurements. The combination of both values will be able to determine an object's material type correctly for most materials. Note that no technology so far can provide the capability of perfect material detection. In general, a technology is considered acceptable if it can provide the capability to detect most of the materials correctly. Using the *density* and Z_{eff} information to determine an object's material type is thus considered a good method.

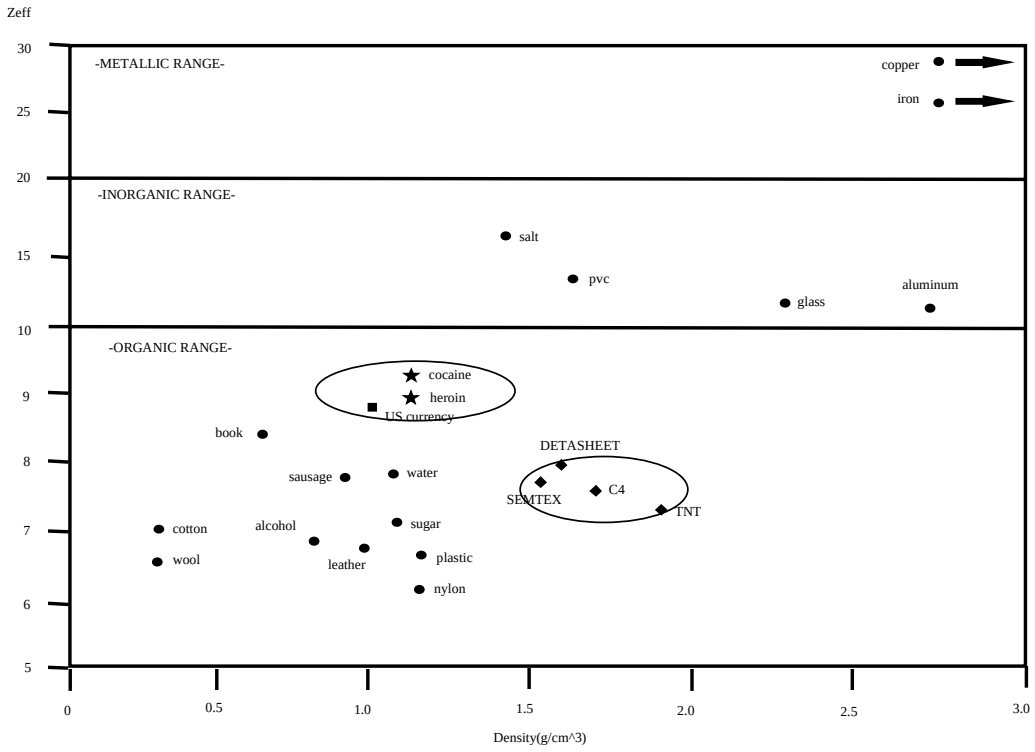

Figure 2.3-1 Z_{eff} and *density* for commonly seen innocuous materials and for illicit materials [EIL92].

2.4 X-ray Sensing Technologies

There are a number of x-ray sensing technologies that can be used for illicit material detection. Those technologies include: single-energy transmission, dual-energy transmission, forward and backward scatter, multiple view, and Computed Tomography (CT).

2.4.1 Single energy transmission

The single energy transmission sensing technology is the most elementary approach to detect illicit materials [FAI92, GRO91, OTA91]. Typically a fan shaped x-ray beam is used as the source, and a line of detectors is used to gauge the amount of x-ray radiation transmitted through the scanned objects. Complete 2-D images are formed by moving the piece of object through the fan beam to create multiple lines of image data. The images produced are fairly high resolution. Consider the x-ray signal obtained in a simple two-dimensional projected image of an inspected object as shown idealized in Figure 2.4-1. The integrated signal, *S*, is simply

$$S = N\log(I_0/I) = N\sigma(N_0/A)\rho ta = \sigma(N_0/A)M \qquad (2.4\text{-}1)$$

where *N* is the number of pixels covering the object's projected area, *a* is the area of each pixel, and *M* is the mass of the material. *S* is a value proportional to total cross-section σ and σ is a function of *Z* or Z_{eff}. *S* is a function of mass, not the *density* one needs to derive. The detection algorithm simply examines the value of *S* of an inspected object. If *S* falls into a certain region, then it is considered to be an illicit material. However, using this method, a small amount of illicit materials or illicit material hidden behind other objects with higher Z_{eff} cannot be detected. This is because in both of these cases, the signal of the illicit material is relatively weak compared to the overall signal from the detection environment due to the large mass of the environment or the large value of cross section.

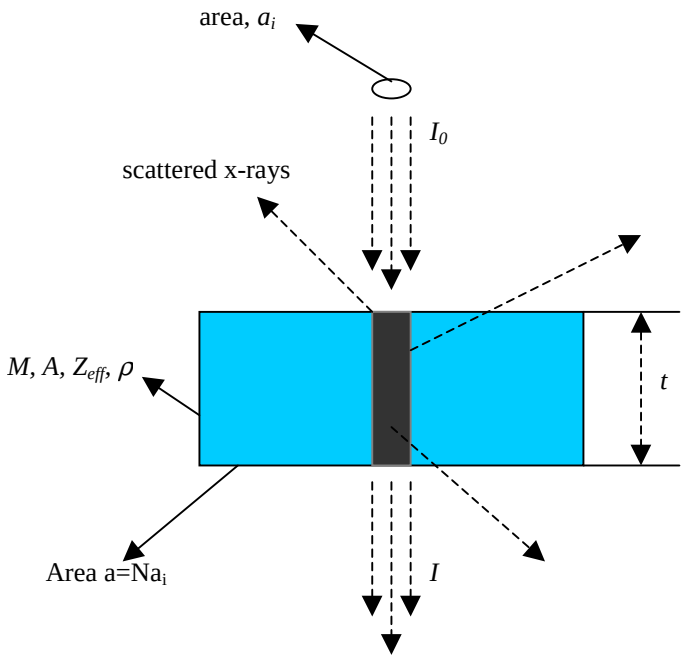

Figure 2.4-1 Illustration of x-ray single-energy transmission technology. The incident x-ray has intensity I_0, the outgoing x-ray has intensity of I. The uniform material has mass M, density r, thickness t, area a, effective atomic number Z_{eff}, and atomic weight A. The area of incident x-ray beam flux is a_i, so that there are $N=a/a_i$ pixels covering the block.

Due to the inherent limitation of this technology, the research and publications on single-energy transmission technology are very few. Most of the research done so far focuses on the dual-energy transmission technology, which can be considered as a significant improvement of the transmission technology.

2.4.2 Dual-energy transmission

Dual-energy systems are really two transmission mode x-ray systems, with beams that are generated by sources that peak at different energies, producing two independent images [FAI92, GRO91, OTA91, KRU94, KRU96]. To determine Z_{eff} and resolve overlapping problem, dual-energy technology can be used. This technology makes use of the fact that the photoelectric effect is strongly Z_{eff} dependent. To see the power and

limitations of this method, assume that only one of the dual-energy transmission technologies is used for inspection; this is equivalent to the single-energy transmission technology illustrated in Figure 2.4-1. Since most dual-energy systems use energy range from 60 keV to 160 keV, the coherent scatter effect can be ignored. Also to emphasize that the incoherent scatter cross section σ_{is} is proportional to Z_{eff}, σ_{is} can be rewritten as $Z\sigma'_{is}$. Thus the total cross sections is the sum of two independent cross sections

$$\sigma(Z_{eff}, E) = \sigma_{pe}(Z^5, E^{-7/2}) + Z\sigma_{is}(E) \tag{2.4-2}$$

in which E is the x-ray photon energy, and $E = hc/\lambda$, where λ is the wavelength, c is the velocity of light, and h is Planck's constant. It follows that

$$\ln\left(\frac{I_0}{I_1}\right) = \left[\sigma_{pe}(Z_{eff}, E_1) + Z_{eff}\sigma_{is}(E_1)\right]\left(\frac{N_0}{A}\right)\rho t \tag{2.4-3}$$

There are too many unknowns in this equation to get much information from a single measurement. In particular, a thin, high Z_{eff} material will have the same attenuation single as a thick, low Z_{eff} material. But two measurements obtained with two different energies can solve part of the problem.

The division of the two signals cancels the common factor of $\mu\rho t$, and the result is

$$R = \frac{\ln\left(\frac{I_2}{I_{20}}\right)}{\ln\left(\frac{I_1}{I_{10}}\right)} = \frac{\sigma_{pe}(Z_{eff}, E_1) + Z_{eff}\sigma_{is}(E_1)}{\sigma_{pe}(Z_{eff}, E_2) + Z_{eff}\sigma_{is}(E_2)} \tag{2.4-4}$$

The ratio shows strong discriminating power at lower energies and heavier Z_{eff}. But there is little discriminating power among the lighter materials. Since E_1 and E_2 are preset and known, using the curve of R vs. Z_{eff}, Z_{eff} can be determined. Figure 2.4-2 shows the curve

of R vs. Z_{eff} for x-ray source low/high-energies at 50/100 keV [ZOU98]. Figure 2.4-3 shows the curve for x-ray source low/high energies at 75/150 keV. The square mark in the graph represents the illicit materials, and the diamond shape mark represents the innocuous materials.

Notice that inorganic materials can be separated from organic materials using R. It can also be observed that the lower the mean of the low-energy x-ray is, the better the discrimination power. The catch is that x-rays with lower energy are usually strongly absorbed and hence in most cases, x-ray beams with energies lower than 40 keV are seldom used. Assume that the x-ray source energies are 75/150 keV, when R is known, Z_{eff} can be computed using the following equation:

$$Z_{eff} = -6.596 \cdot 10^5 e^{-9.815R} + 4.685 e^{0.6783R} \qquad (2.4\text{-}5)$$

All the equations presented thus far have assumed the x-ray source is monochromatic. Therefore the thickness and density factors can be canceled out. However in practice, most x-ray sources are polychromatic. For polychromatic x-ray sources, the thickness and density factors will not be canceled out, so the R and Z_{eff} relationship is much more complicated. To determine what this relationship is, usually MCNP simulations or experimental measurements are used. MCNP is the abbreviation for Monte Carlo N-Particle. It is a simulation software package developed at Los Alamos National Laboratory to simulate neutron, photon, and electron transport [LOS93]. Ms. Wei Xie has demonstrated that MCNP is quite precise in simulating the interaction between x-ray beams and matters [XIE95].

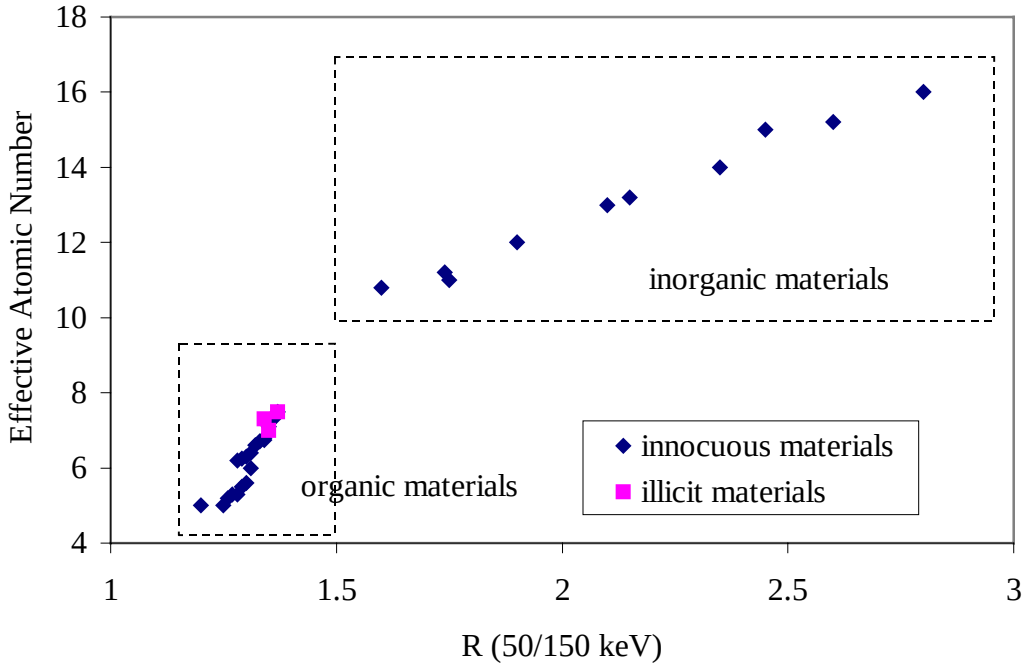

Figure 2.4-2 *R* vs. Z_{eff} for x-ray source low/high energy 50/100 keV [ZOU98].

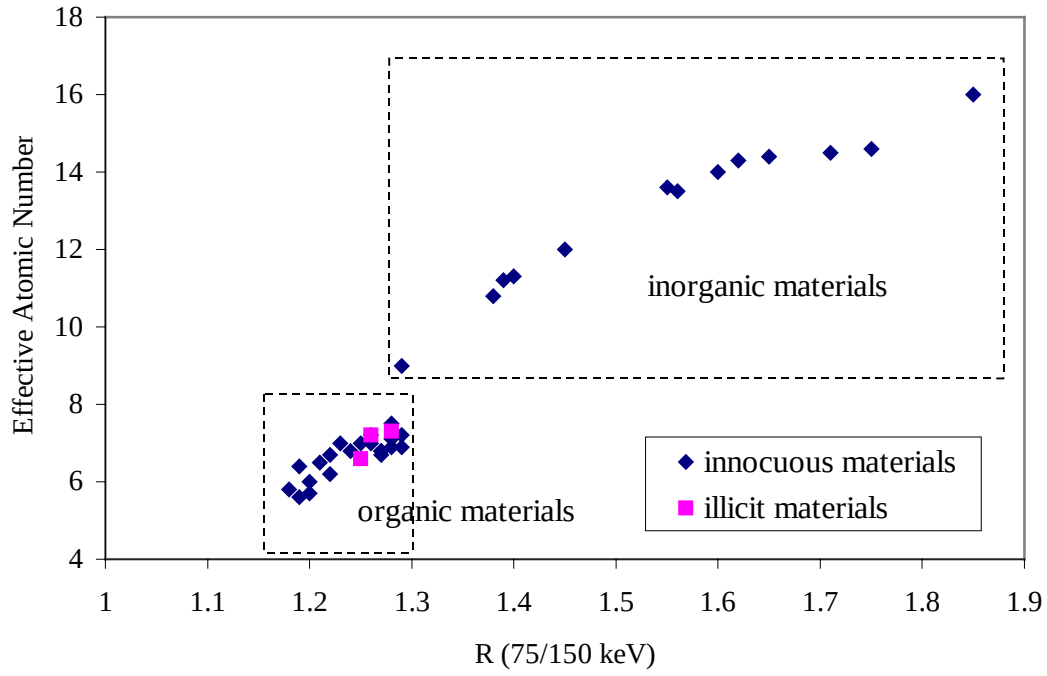

Figure 2.4-3 *R* vs. Z_{eff} for x-ray source low/high energy 75/150 keV [ZOU98].

There are two types of dual-energy systems: pseudo dual-energy systems and true dual-energy systems. A pseudo dual-energy system uses a single x-ray source and two sets of detectors mounted one behind the other. The setup is seen in Figure 2.4-4. The x-ray source is set to a constant voltage. The detector located nearer to the x-ray source receives the x-ray beam and absorbs the low energy part of the x-rays. After passing through the copper filter, the low energy part of the x-ray is significantly reduced. The second detector absorbs the remaining high energy x-rays.

The spectral response of the high- and low-energy detectors is plotted in Figure 2.4-5 [XIE95]. It is known that the further the two response curves are separated from each other, the better the detection result. The purpose of this copper filter is to reduce the amount of energy in the low-energy region so as to further separate the spectrum distribution of the low- and high-energy detector response curves. As should be relatively clear, one problem with pseudo dual-energy systems is that the intensity of the filtered high-energy x-rays reaching the second detector is significantly reduced by the filtering process. Hence the high-energy signal has more noise than that of a true dual energy system.

There are two types of settings for a true dual-energy system. One type of setting uses one x-ray source and one detector, and the operation is done by scanning the inspected objects twice. On the first run the x-ray source is set to a low-energy level and a low-energy image is obtained. On the second run the x-ray source is set to a high-energy level and the object is scanned again, the high-energy image is obtained. [GRO91, ZOU98]. The modified AS&E 101ZZ system used in my experiments belongs to this type of settings.

Another type of setting uses two x-ray sources and two detectors. One source is set at a high-energy level; another source is set at a low-energy level. The inspected object first passes through the high-energy x-ray source and then passes the low-energy x-ray source, the high- and low-energy images are obtained. The system developed by Heimann Inc. uses this type of setting.

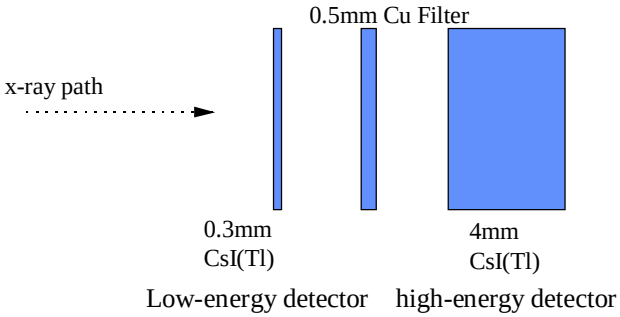

Figure 2.4-4 Side view of a pseudo dual-energy x-ray detector [XIE95].

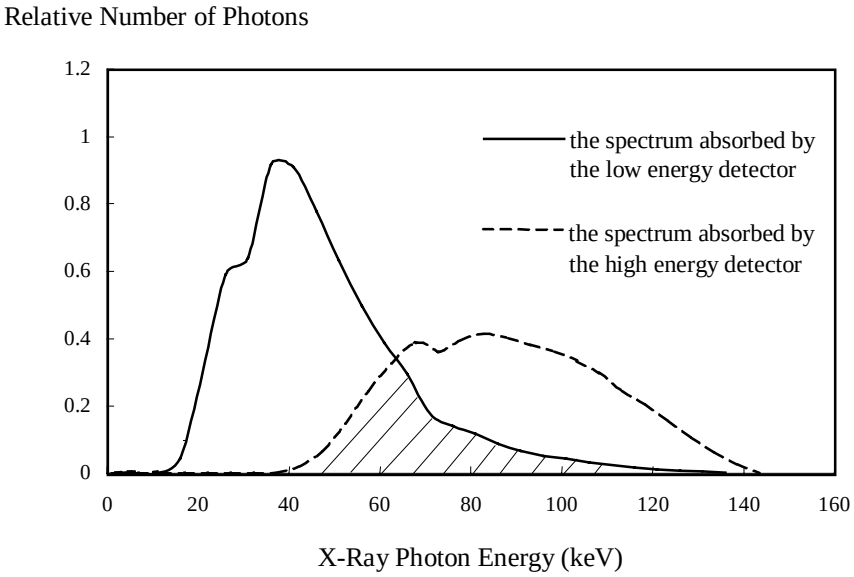

Figure 2.4-5 Spectrum response of the high- and low- energy detectors [XIE95].

As said earlier, the modified AS&E 101ZZ system is used for image collection. To improve the performance of the dual-energy system, some work was devoted to investigate the energy distribution of this AS&E 101ZZ system. Figure 2.4-6 shows the energy distribution curve for a one-source x-ray true energy system [DRA98]. There is a large overlapping area between the low-energy and the high-energy x-ray curves. Theoretically, the larger the degree of separation between the low and high in terms of distributions the better. Apparently some measurements need to be taken in order to decrease the overlapping area and to increase their degree of separation. This was done by inserting a copper filter in front of the detector when the high-energy x-ray beam is used.

Figure 2.4-7 shows the variation of energy spectrum after the insertion of a copper filter with different thickness from 0.5 mm to 2 mm. In this graph, S_{80} is the energy distribution curve when x-ray source energy is set to 80 keV. S_{150} is the energy distribution curve when x-ray source energy is set to 150 keV. $S_{150,t}$ is the energy curve when a copper filter with thickness of t mm is inserted in front of the detector. As one can see, the larger the degree of separation of the energy distribution curve is, the smaller the total energy that is under the high-energy x-ray curve. Dual-energy system performs better with large degree of separation of the energy distribution curve; it also performs better when the total energy under the high-energy distribution curve gets larger. Those two goals apparently are conflicted to each other. Mr. Xinhua Shi has been able to come up with a cost function that tries to determine the thickness of the copper filter to achieve the best detection result. He has proven that when t is 1 mm, the material characterization result is optimized [DRA98]. The discussion of this work is quite complex, and is beyond the discussion of this dissertation. Mr. Shi will give detailed discussion of the copper filter in his dissertation that is currently in preparation.

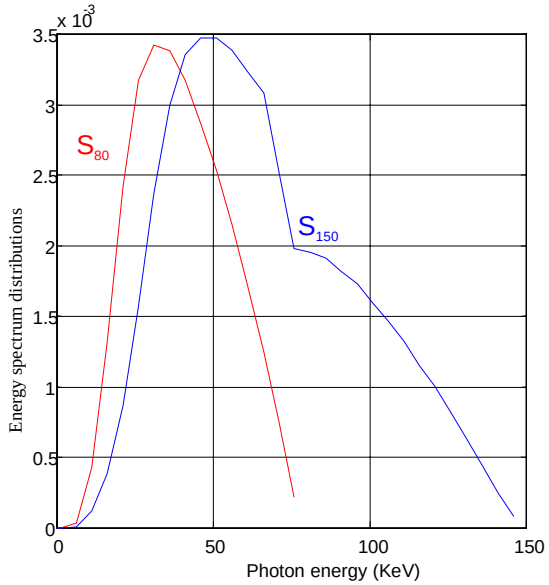

Figure 2.4-6 Energy spectrum of an X-ray tube that produces true dual-energy x-ray beams [DRA98].

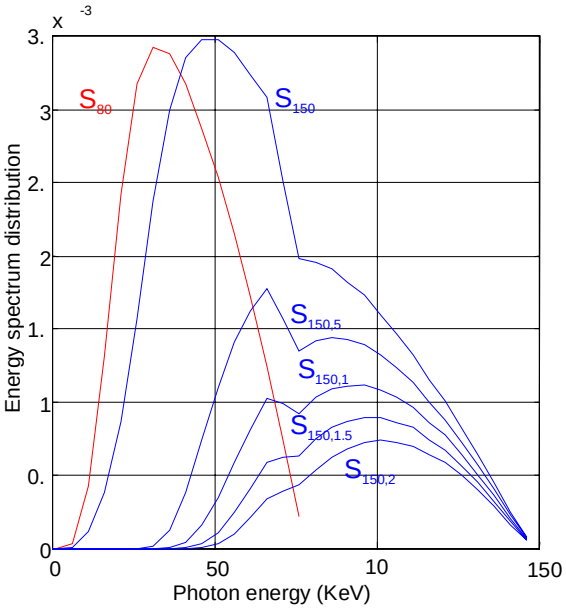

Figure 2.4-7 Variation of energy spectrum after inserting a copper filter.

There are few occasions that one can use Equation 2.4-4 to directly derive Z_{eff}. This is because the contents of a detection environment are infinitely varied and only occasionally neatly placed; and illicit materials are always camouflaged when they are transporting. When Equation 2.4-4 is directly applied to the detection environment, it no longer gives the Z_{eff} of the object that is intended to detect, rather it gives the mixture of the material and its overlapped background objects.

There are several methods to resolve this problem. One algorithm developed by Vivid Technologies [KRU94, KRU96] found a partial solution to eliminate the background overlapping object effect using one-view dual-energy transmission technology. First, a characteristic value K_{MAT} is computed for each illicit material. K_{MAT} is computed from the attenuation coefficients of the illicit material in high- and low-energy respectively. The algorithm then starts by examining the image on a pixel by pixel basis. For a test pixel, a value K_{TB} is computed for each pair of pixels; a pair of pixels is composed by the test pixel and a nearby pixel that is considered to be its background. The test pixel counter is incremented by one if K_{TB} is equal to K_{MAT} of any illicit material. If the counter number for a test pixel is greater than a certain threshold, this pixel is considered as belonging to an illicit material. K_{TB} is computed using

$$K_{TB} = \frac{\ln\left(I_T^H\right) - \ln\left(I_B^H\right)}{\ln\left(I_T^L\right) - \ln\left(I_B^L\right)} \tag{2.4-9}$$

where I_T^H and I_T^L are signals of the test pixel in high- and low-energy bands respectively; I_B^H and I_B^L are signals of the background pixel in high- and low-energy bands respectively. Equation 2.4-9 is believed to have the power of eliminating the overlapping background effect. There is a serious flaw in this algorithm. Using this algorithm, the background pixel selected is usually a neighboring pixel of the test pixel. Unless the test pixel is on a boundary between an object of interest and its background object, the background pixel selected is not its real background. The system using this algorithm has a very low detection accuracy.

Another method, which is first developed by Hologic Incorporation [STE91] and further improved by Vivid Technologies Incorporation [KRU97], is claimed to be a very effective algorithm for attacking the overlapping problem. This algorithm is applied to four images that are obtained by using high- and low-energy x-ray beams. Two images, the low- and high-energy images are obtained with no reference material being present. The final two images are low- and high-energy images with the reference material present. This is illustrated in Figure 2.4-8. Let the two images produced without reference materials be denoted as I_h and I_l, and let the two images produced with the reference materials be denoted by I_{rh} and I_{rl}. The reference material is made of the illicit material one intends to detect.

For each image pixel, a value k is computed based on the values from those four images, where k is given by

$$k = \frac{L_r - L}{H_r - H} \tag{2.4-10}$$

where $H_r=log(I_{rh})$, $H=log(I_h)$, $L_r=log(I_{rl})$, and $L=log(I_l)$. Since k is the ratio of the attenuation coefficients at low- and high-energy, it is approximately independent of thickness. k depends only on the Z_{eff} of the reference material. A new value Q is then computed for every pixel of the image, where

$$Q = L - kH\ . \tag{2.4-11}$$

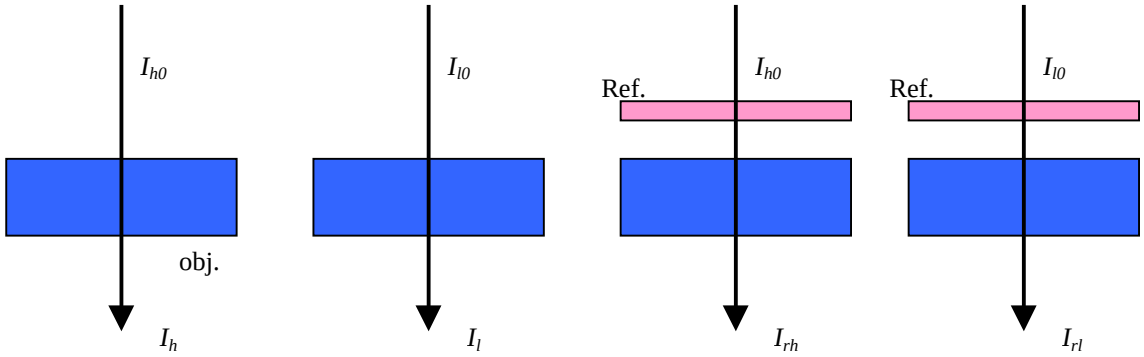

Figure 2.4-8 Illustration of obtaining four different images I_h, I_l, I_{rh}, and I_{rl} by using dual energy x-rays with and without a reference material.

Q is then used to form a two-dimensional array, which is a new image. This new image is different from the original image because the objects that have the same Z_{eff} as the reference material are no longer shown in this image. They disappear from view. If the reference material happens to be made of a certain type of illicit materials, the objects no longer appearing in Q will have very high probability of being an object made from the same material as the reference. The detection accuracy of this algorithm can be precise if all the known illicit materials were referenced when producing the images. Unfortunately, to do so requires that a very large number of scans be taken. This is impractical for real-time operation.

An alternative approach to this algorithm is given in another patent [KRU97] developed by Vivid Technologies. Reference materials are not used in this approach; instead, only high- and low-energy images are collected. Vivid Technologies claims that this approach can precisely determine Z_{eff} even under severe overlapping cases. However, this patent does not disclose the details of the detection algorithm employed; rather it only describes the functionality of this procedure. The claims state that the algorithm has successfully

improved the detection accuracy because the algorithm has given full consideration of the polychromatic nature of the x-ray source, unfortunately no details or any other proofs are presented in this patent to substantiate this claim.

In summary, single-view dual-energy systems can determine Z_{eff} of an object. Some algorithms do have the partial capability of determining Z_{eff} even when object overlap occurs. None of the systems can determine an object's *density*. Without *density* information, innocuous organic materials such as food cannot be distinguished from illicit materials. The algorithms are still primitive, and no sophisticated image processing algorithms are used to improve the detection accuracy.

2.4.3 Multiple views

An existing multiple-view system usually uses single or dual-energy transmission technologies [BJO92]. It uses two or three orthogonal views to obtain several 2-D images to reconstruct a 3-D model of the scanned object. There are two reasons for developing this type of system — to obtain more precise Z_{eff} and to obtain some *density* information. In a 2-D image, when objects are overlapped, the properties of the object of interests are often mixed with those of its background objects. With a second or even a third view, a 3-D model can be constructed. An object that is overlapped with other background objects can be separated from its background objects. An object that is hidden behind other objects in a 2-D image can also be revealed. Since a 3-D model can be reconstructed, volume information can be obtained. The *density* of an object can be determined using this volume information. Figure 2.4-9 shows a setting of a two-view system [GRO91].

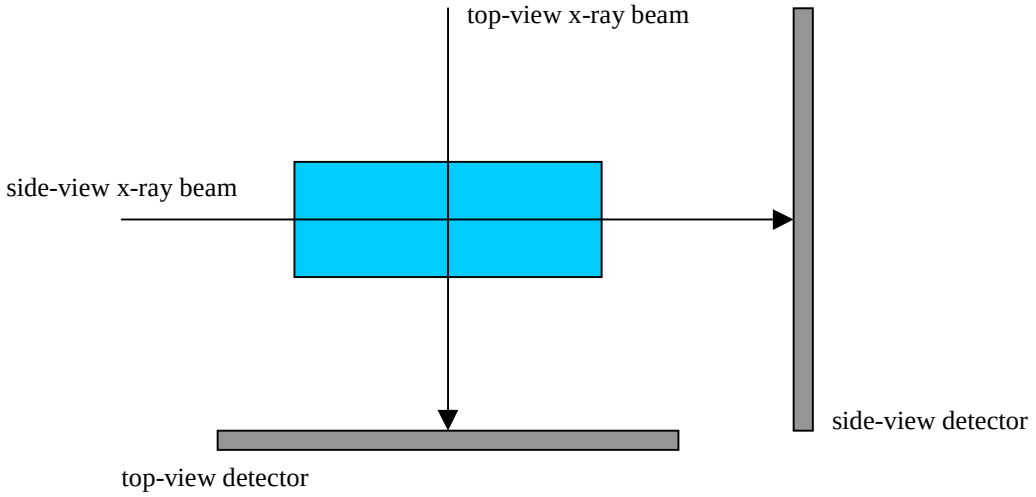

Figure 2.4-9 Schematic of a two-view system using two separate x-ray sources and detectors arranged orthogonally.

One such system has been developed is an EG&G Z-scan system by EG&G [BJO92]. It uses a Multiplicative Algebraic Reconstruction Technique (MART) to construct two 2-D images into one 3-D image in rapid convergence. However, many false reconstruction results are made using MART because two views still contain ambiguities and degeneracy. The more views that are taken, the less the ambiguities, but the running time of the reconstruction algorithm will go significantly higher.

2.4.4 Computerized Tomography

Computer Tomography (CT) machines can create three-dimensional images of a luggage bag [EIL91, ROD91]. They do so on a slice-by-slice basis. To create each slice over a hundred or more line scan views of a bag are taken, each from a different direction. The information contained in these views can then be used to reconstruct the three-dimensional structure of the bag in the imaging plane from which all the views were taken. As such these machines literally unpack a container electronically and can examine object composition regardless of overlapped objects. Theoretically they have much more capability of precisely measuring the *density* of objects in bags and if dual energies are used in taking the view, they can more precisely estimate Z_{eff} as well. Such a dual-energy CT machine would be about to directly address the Z_{eff} vs. *density* map shown in Figure 2.3-1. The demerits of those systems include their slow processing speed, high cost, large size, and high x-ray dose needed to inspect a bag. In recent years, major advances have been reported for the time required to process and examine individual slices. However, the overall time needed to thoroughly process and examine a container with hundreds of slices still limit its usefulness as a front-line, rapid inspection device. Figure 2.4-10 to Figure 2.4-14 show the 3-Dimensional reconstruction of a suitcase [SHR91]. Figure 2.4-10 shows the viewpoint for the reconstruction. Figure 2.4-11 shows a reconstructed layer that is 3 inches above the bottom of the suitcase. Figure 2.4-12 shows a reconstructed layer that is 2.3 inches above the bottom of the suitcase. Figure 2.4-13 shows a reconstructed layer that is 2 inches above the bottom of the suitcase. Figure 2.4-14 shows a reconstructed layer that is 0.3 inches above the bottom of the suitcase.

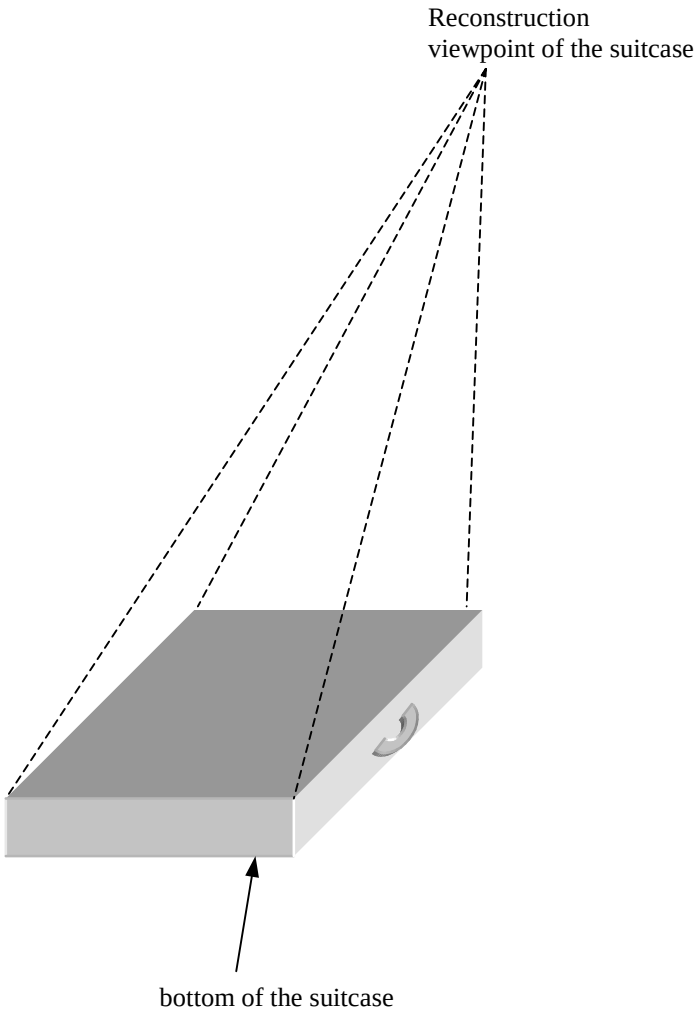

Figure 2.4-10 Illustration of the viewpoint of a 3-D reconstruction of a suitcase.

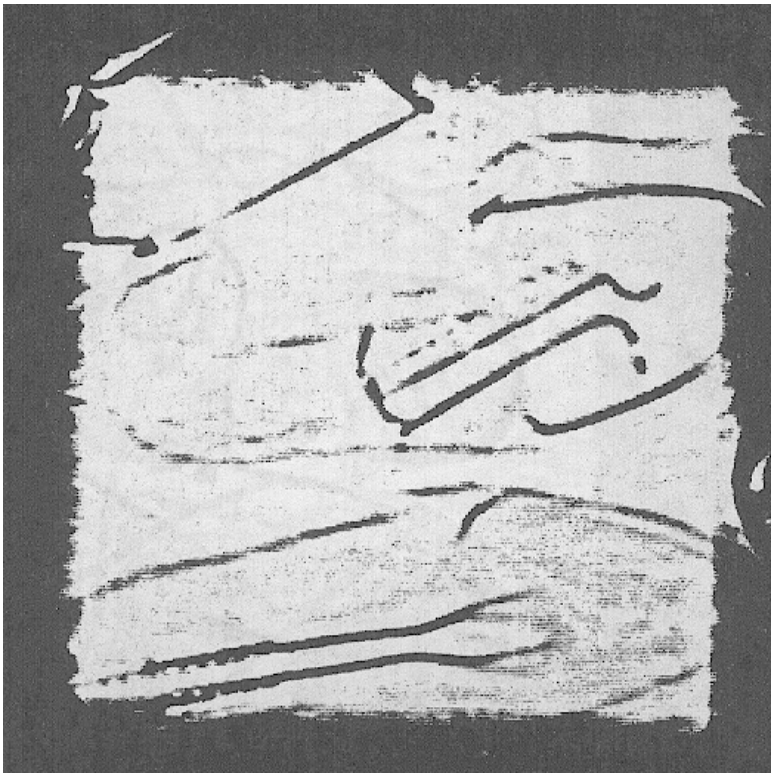

Figure 2.4-11 Reconstructed layer that is 3 inches above the suitcase bottom. The shoe trees and the top of the aerosol can be visible [SHR91].

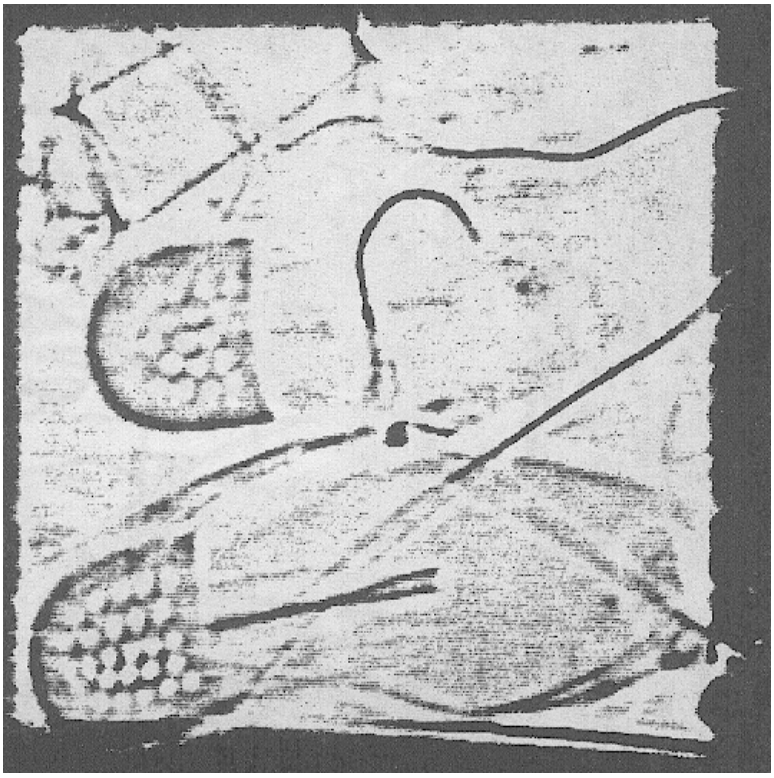

Figure 2.4-12 Reconstructed layer that is about 2.3 inches above the suitcase bottom. The heels of the shoes, coat hangers, and aerosol are visible [SHR91].

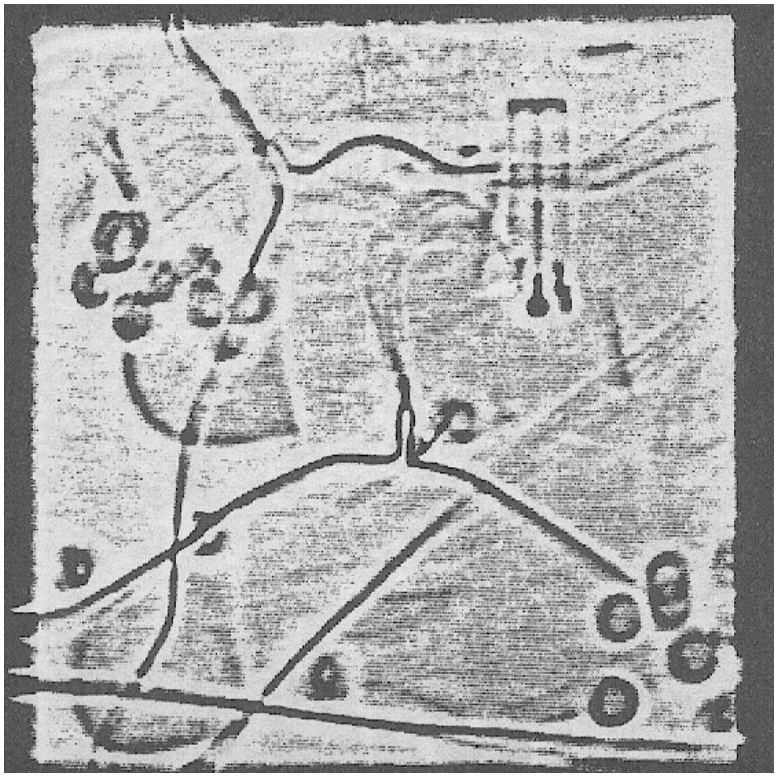

Figure 2.4-13 Reconstructed layer that is about 2 inches above the bottom of the suitcase. The coat hangers, coins, and a cigarette lighter are visible [SHR91].

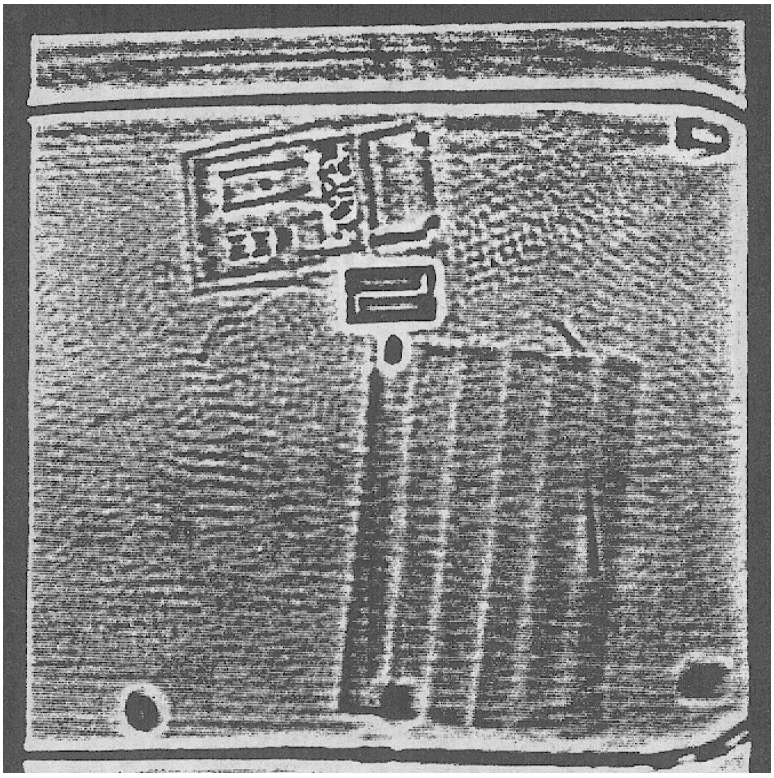

Figure 2.4-14 Reconstructed layer that is 0.3 inches above the bottom of the suitcase. The simulated explosive, a battery pack, a pocket calculator, and wires are clearly visible [SHR91].

2.4.5 Forward scatter and backscatter

There are two types of scatter detection technologies: one is to measure the coherent scatter [STR93, SPE93], and the other is to measure the Compton or incoherent scatter [FAI92, GRO91, OTA91, KRU91].

Coherent scattering

Coherent scatter that occurs can be measured by a setup shown in Figure 2.4-15 [STR93]. A pencil-beam is formed by an x-ray tube and a collimator, and the beam is scattered by the inspected object. A scatter collimator is used to confine the scattered signal and only the photons with a scatter angle Θ of 3 degrees can reach the detector.

The coherent photon scattering process is characterized by the conservation of energy of the photon while its momentum vector changes direction. By measuring the momentum vector changing, the energies of the scattered x-ray photons can be computed. This energy is a function of the molecular lattice spacing present in the scatter material. The energy spectrum of coherently scattered x-rays therefore will exhibit peaks, with *positions* corresponding to the *lattice spaces* and with *integral heights* corresponding to the *number of scatter centers* in the scatter voxel. The *peak widths* indicate the degree of local atomic (or molecular) *disorder*. Explosives or their constituents exhibit elastic x-ray spectra with pronounced peaks in the energy range between 30 and 100 keV. The number of peaks, their positions, heights, and widths have shown to be characteristic features for their identification.

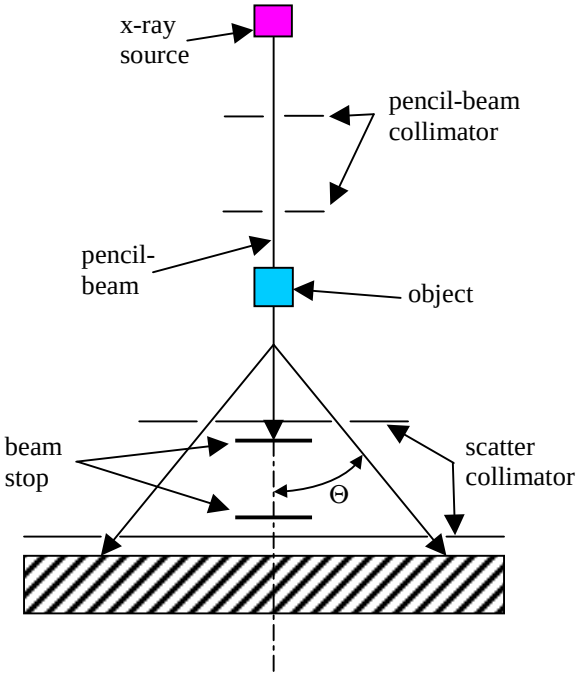

Figure 2.4-15 Schematic drawing of a pencil-beam elastic x-ray scatter system [STR93].

To determine an object's material type, the prominent scatter peaks of this object's spectrum are compared against the prominent peaks of known materials. If all peaks of this object match all peaks of a known material, this object's material type should be the same as that known material. The coherent scattering measuring technology directly extracts material characteristics regarding the crystalline structure of bulk objects. The detection result is not affected by the incident x-ray spectrum. This technology can also be run in real time, and the detection accuracy is relatively high.

However, there are several demerits to this technology. The detection of a material is based on a match between the detected scatter spectrum and the "pattern" of the known material within a specific window. If a material is mixed with another material, and/or is located in a complicated detection environment, the scatter spectrum of a material may be different from when it is only surrounded by air. This change obviously affects the accuracy of the window comparison method. It is also very difficult to determine the "pattern" for identifying a specific material. The penetration power of the coherent signal usually is very weak; thus it is very difficult for thick bags to generate high quality coherent scatter images. For these reasons, this technology has not been used widely in practice.

Incoherent scattering

The second method is to measure the incoherent or Compton scattering. In most cases, forward scatter and backscatter are measured using two scatter detectors, as seen in Figure 2.4-16. Compton scattering is the dominant mode of interaction for most materials in the photon energy range from 0.3 to 2.0 MeV [ARE96]. Moreover, the probability of Compton scattering is directly proportional to the electron density, N_e, which is related to the mass density, ρ, by the relationship:

$$N_e = \frac{Z_{eff}}{A} \rho N \qquad (2.4\text{-}12)$$

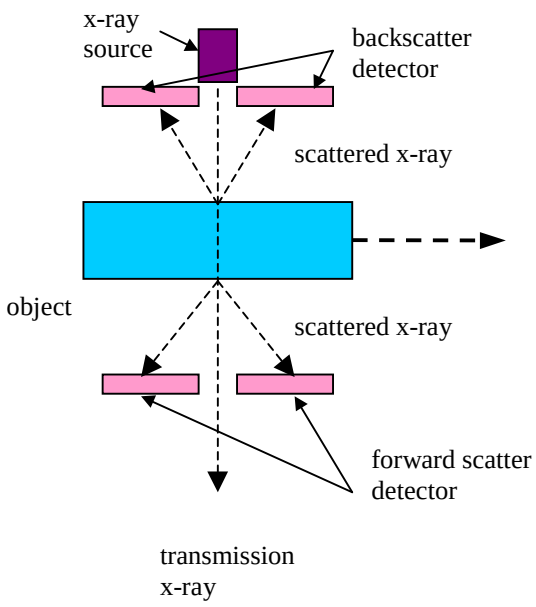

Figure 2.4-16 Illustration of obtaining x-ray forward scatter and backscatter images.

where A is the atomic weight and N is Avogadro's number. For most materials, Z/A is equal to about one-half; therefore, the electron density is indicative of the mass density. This makes the Compton scattering signal get stronger as the mass density increases. It also makes Compton scattering a natural choice for deriving *density* information about objects.

Compton scattering from high Z materials is suppressed by the photoelectric attenuation. The scattered intensity I_{is} from a sheet material into a detector that subtends Ω of a sphere is given by:

$$I_{is} = I_0 \Omega \left[1 - e^{-\sigma m t}\right] \frac{\sigma_{is}}{\sigma}. \qquad (2.4\text{-}13)$$

Though this equation has established the relationship between partial scatter signal (such as forward scatter and backscatter) and total scatter signal Ω is in reality difficult to compute.

Because of energy conservation, the energy of the scattered photon is reduced by the recoil kinetic energy of the struck electron. For 100 keV x-rays, the scattered photon is reduced energy by nearly 40 percent [FAI92]. The scattered photons, which are being so reduced in energy, cannot penetrate a material as deeply as the energetic incident beam. Consequently both the forward scatter and backscatter detectors are typically used for detecting illicit materials located in or near the surface of the bags. The advantage of backscatter is obvious. Since the source and the detector can be placed at the same side of detecting objects, many applications depending on this particular setting are created, such as the inspection of cargo vehicle.

One important observation is that the Compton scattering signal will get stronger if the material has lower Z_{eff}, higher density, and shorter distance to a bag's surface, and vice versa [ANN92]. Most illicit materials, especially plastic explosives, have low Z_{eff} and are high in density. It is fair to say that this technology gives much more information about

low *Z* material in the near surfaces of a bag than is otherwise impossible to obtain. Using this technology, AS&E Technologies Incorporation [ANN92] and Vivid Technologies Incorporation [KRU97] have both created system to detect illicit materials in general and plastics explosives in particular.

This discussion is focuses on the AS&E system since Vivid Technologies has not yet disclosed the details of their algorithms. The AS&E system is actually a multisensing system; the system can obtain a transmission image and a backscatter image simultaneously using a flying spot scanner. The design details will be given in the next chapter. Instead of using a pixel-by-pixel image processing analysis, AS&E has devised a cumulative histogram analysis technique to identify the existence of illicit materials. The analysis is performed on both of the scatter and transmission x-ray images. From the backscatter image, a special histogram H_i is computed. H_i is defined by

$$H_i = \sum_{j=1}^{512} \sum_{k=1}^{512} f_{j,k(i)} \tag{2.4-14}$$

where

H_i = number of pixels with brightness greater than i. (2.4-15)

$$f_{j,k(i)} = \begin{cases} 0 & \text{if the scatter value of the } j^{th} \text{ pixel of the } k^{th} \text{ row is less than i.} \\ 1 & \text{if the scatter value of the } j^{th} \text{ pixel of the } k^{th} \text{ row is greater than i.} \end{cases} \tag{2.4-16}$$

A typical scatter histogram is shown in Figure 2.4-17.

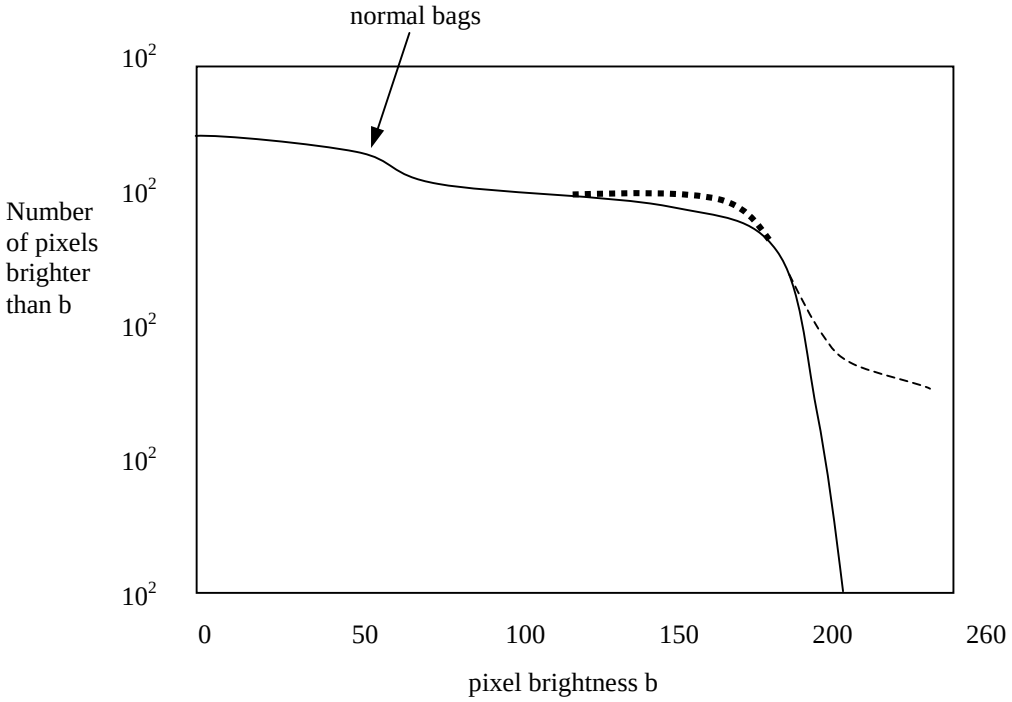

Figure 2.4-17 Typical threat curve (solid line) and the regions of the histogram where a bag would exceed the threat curve if it contained either a compact bomb (dashed line) or a sheet bomb (dots).

The EG&G detection algorithm is based on the fact that if a bag had an illicit material hidden within it, the object would show up in the image as a region of intense scatter. In the histogram H_i, it would appear as a significant increase in the number of pixels having at high scatter level. This feature is shown as a dashed line in Figure 2.4-17. If, however, a sheet explosive bomb were present, it would appear as a small increase in scatter over a large number of pixels. This is shown as a dotted line in Figure 2.4-17. Note the normal luggage bag curve is shown by a solid line. Using this algorithm, the bag size, density, and type variations must be considered.

Note the above described algorithm is only a simplified version of the actual method used for finding bombs. The actual system uses both the transmission and scatter histograms to define a large variety of illicit materials that may be present in the detection environment. The accuracy of this algorithm is comparable to the dual-energy system; however, its unique capability of detecting sheet explosives on the bag's surface and deriving *density* related information make this technology as one of the most promising technologies for detecting illicit materials.

2.5 Deriving Z_{eff} and *Density* Information

From the surveys in Section 2.3 and Section 2.4, we know that x-ray technology relies on determining an object's *density* and Z_{eff} characteristic values to determine an object's material type. From the research I have done so far, it seems that there is no single sensing technology that can provide all the needed information for determining a material's Z_{eff} and *density* [FAI92, GRO91, NAS91, OTA91, OTA92]. An improvement to this is to use multisensing technologies to determine an object's material type. However, all the existing multisensing systems are so called "pseudo-multisensing systems." They are multisensing systems because their systems have been equipped with several x-ray technologies for illicit material detection. Those systems are "pseudo-multisensing systems" because the detection of a single type of material utilizes only one technology. For example, the system developed by Vivid Technologies uses both the duel-energy transmission and scatter technologies for illicit materials detection. But the

duel-energy transmission is responsible for regular illicit material detection, while the scatter technology is responsible for sheet explosive detection only. In conclusion, most current x-ray systems only use either Z_{eff} or *density*, but not both to determine the material type. The determination accuracy inevitably will be degraded by insufficient information obtained from the method.

An alternative is to use data-fusion techniques so that all the information combined will be integrated together to arrive at the detection result. In other words, a true multisensing system is needed to improve the detection accuracy. The technology combination chosen in this dissertation is dual-energy transmission technology plus scatter technology (forward and backward). Those two technologies are chosen because those two types of technologies are the most commonly used technologies in existing systems. The technologies are sophisticated and are relatively inexpensive. In addition, both technologies can inspect objects in real-time. The multisensing system built based on those two technologies should be also inexpensive, sophisticated, and have the potential to inspect objects in real-time. Dual-energy transmission technology can provide Z_{eff}-related information about a material, and scatter technology can provide *density*-related information. Since both Z_{eff} and *density*-related information are known, the detection results should be more precise.

One-view system is the focus of discussion because I believe that this one-view system provides data accurate enough to determine an object's material type. A two-view system will also be briefly discussed in this dissertation, mostly because I feel that adding a second view in order to obtain the object's thickness and distance information will further improve the performance of the proposed system.

2.5.1 Deriving *density* information

In previous sections, I have shown that using dual-energy transmission scanning technology, Z_{eff}-related information can be derived, and that using scatter imaging technology, *density*-related information can be derived. If both these pieces of

information are available about a material, the type of the material can theoretically be more accurately determined. In dual-energy transmission systems, Z_{eff} can be derived from R using Equation 2.4-5, and R can be computed using Equation 2.4-4. Since R has a one-to-one mapping relationship to Z_{eff}, there is no real need to compute Z_{eff} from R. R itself is a characteristic value that can be used to determine the material type. I have demonstrated in Section 2.4.2 that R can be used to separate organic materials from inorganic materials and metals. Now it is necessary to study the method by which *density*-related information can be derived.

In Section 2.4-5 it was shown that scatter data can be used to derive the *density*-related information. After careful study by Ms. Shubin Zou and I [ZOU98], it was found that by using value L (a value named after my initial), the *density*-related information can be revealed. L is computed from the observed scatter and transmission signals, and is defined as follows:

$$L = \frac{I_{sc}}{I_{tr}} \tag{2.5-1}$$

where I_{sc} is the scatter signal and I_{tr} is the transmission signal. It should be pointed out that theoretically, I_{sc} is the combination of the incoherent scatter signal I_{is} and the coherent scatter signal I_{cs}. In practice, since only the forward scatter signal I_{fs} and the backscatter signal I_{bs} can be measured, but not the scattered x-ray photons at other directions, I_{sc} can only be estimated as

$$I_{sc} \approx aI_{fs} + bI_{bs} \tag{2.5-2}$$

where a and b are two factors intended to minimize the distance effect on the total scatter signal. The significance of those two factors will be described later in this section.

Using L, denser organic materials can be separated from less dense materials, as seen in Figure 2.5-1. Denser materials are materials like explosives and drugs. Less dense

materials are materials like innocuous organic materials. The data shown in Figure 2.5-1 were obtained from a number of MCNP simulations. In these simulations, the x-ray source energy spectrum is assumed to have the same characteristic as an AS&E 101ZZ system x-ray tube. The sizes of both the forward scatter and backscatter detectors are the same. Each detector is assumed to be 56 cm in width and 50 cm in height. This size happens to be the same size as that of the modified AS&E system – the system that was used to collect data for this study. The energy of the x-ray beam used is 75 keV. This simulation data is produced assuming that the thickness of all materials is 0.1 cm. The factors *a* and *b* are both set to 1.

It is now necessary to explain what the constants *a* and *b* represent. When an inspected object is placed between an x-ray source and a scatter detector, the distance between the object and the detector affects the measurement of the scatter signal. For example in Figure 2.5-2, an object is placed closer to the forward scatter detector in case (a) than in case (b). When this happens, the sphere subtends by θ_{fs} and is larger in case (a) than in case (b).

Since the scattered photons will be in all directions, the forward-scatter detector in case (a) receives stronger signals than in case (b). The result becomes distance dependent. Fortunately, when this object moves closer to the forward scatter detector, the distance between the backscatter detector and the object becomes greater; consequently the backscatter detector will receive weaker signals. It is desired to find a method to make the estimated scatter signal independent of the object's distance from the two detectors. Using adaptive modeling method, Mr. Xinhua Shi came up with two values that basically satisfied this requirement: constant *a* should be set to 1; constant *b* could be set to any value between 1 and 1.2. Please note that this part of the research is still an on-going activity. Mr. Shi will summarize his research results in his Ph.D. dissertation that is current in preparation.

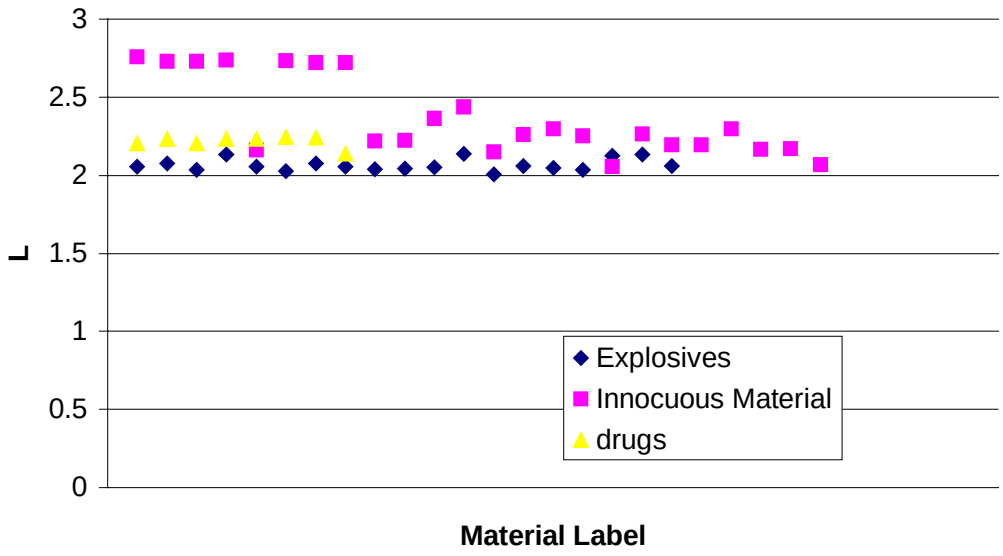

Figure 2.5-1 Illustration of using *L* to discriminate denser materials from less dense materials.

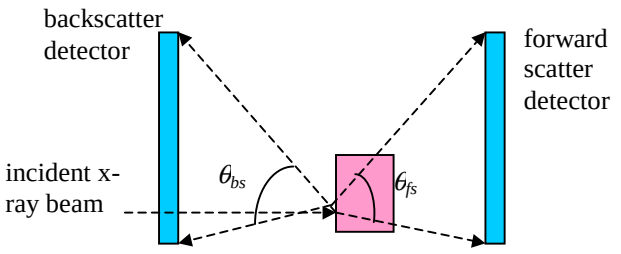

(a)

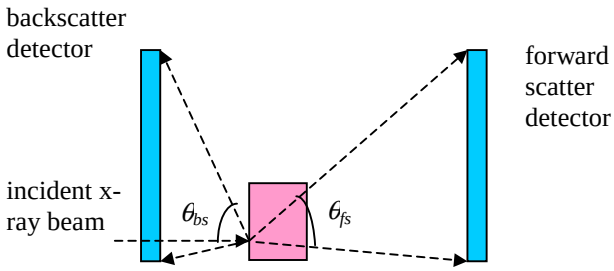

(b)

Figure 2.5-2 Illustration of how the distance factor affecting the strength of scattered signals.

2.5.2 Using *R-L* values to determine material type

As has been discussed previously, using a combination of *L* and *R* measurements should be more precise in determining an object's material type than just using a single characteristic value. To verify this conclusion, a simulation was done using the materials listed in Table 2.1-1. In this simulation, the transmission detector geometry is assumed to be an ideal round shape detector with a diameter of 0.5 cm. The energy of the x-ray source is set to 150 keV for high-energy detection, and 75 keV for low-energy detection. In these simulations the forward and backward scatter signals are obtained when the source is set at low energy setting of 75 keV. The object's thickness varies from 0.1 cm to 10 cm. Once a material's transmission, forward scatter, and backscatter signals are obtained, *R* and *L* are computed for this material. The results are plotted in an *R-L* plane, as seen in Figure 2.5-3. "+" denotes explosive, "o" denotes drugs, and "Δ" denotes innocuous organic and inorganic materials. What are shown in this graph are innocuous materials that are easily mixed up with illicit materials and those illicit materials. Metals were not plotted in this graph, because using *R* alone metals can be separated from other materials. There are also many inorganic and organic materials that can easily separated from explosives and drugs using *R-L* plane, and they are not drawn in this graph. It can be seen there is a clear boundary between explosives and innocuous materials. However, such a clear line does not exist for drugs. Fortunately this dissertation focuses on the detection of explosives material, so the accuracy of *R-L* plane method is satisfied.

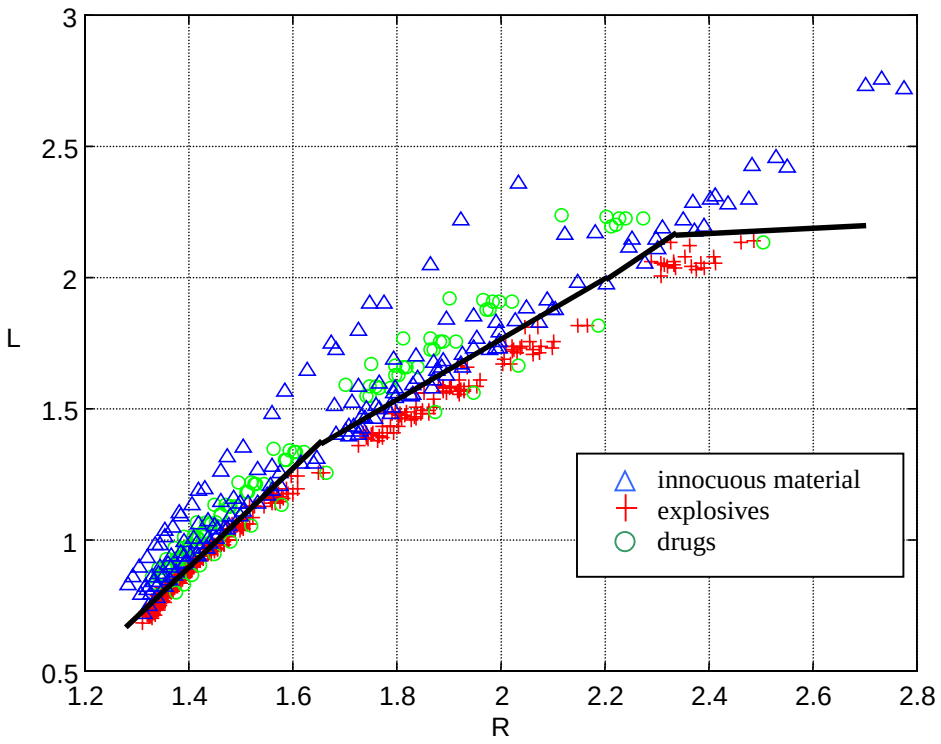

Figure 2.5-3 Explosives, drugs, and some selected innocuous materials on the *R-L plane*.

2.6 The Proposed Study

2.6.1 The goal of study

To use the *R*-*L* plane to characterize an object's material type, one must be able to infer what the object's *R* and *L* values actually are. However, the *true R* and *L* values of an object can only be computed using this object's *true* gray levels in both dual-energy transmission and scatter modalities. The *true* gray levels can be explained as follows: when an object of interest is placed in air, and there is no background objects appearing, the gray level measured is called the *true* gray level of this object. Since multisensing technologies are used, a *true* gray level is measured for this object in each of the sensing modality. The set of *true* gray levels that are being measured in all sensing modalities is simply referred to as the *true* gray levels of this object.

The *true* gray levels are not easy to compute because an object of interest is often seen ***overlapped*** with several background objects in a bag environment. This is illustrated in Figure 2.6-1. The object of interest can be seen overlapping with a background object. When this happens, the transmitted signal is the strength of signal after the x-ray beam traverses through the object of interest and its background object. The forward-scattered and backscattered signals measured are also the combined effects caused by those two objects. The strengths of the signals measured are very different from the strengths of signals when the incident x-ray beam passes through only the object of interest. It is known that value *R* is computed using the transmitted signals, and value *L* is computed using the low-energy transmission signal along with the forward scatter and backscatter signals. Those two values reflect the material properties of the combined effects of the object of interest and its background objects. They do not reflect the material property of the object of interest. Using this measured *R* and *L* to determine the material type of the object of interest is simply meaningless.

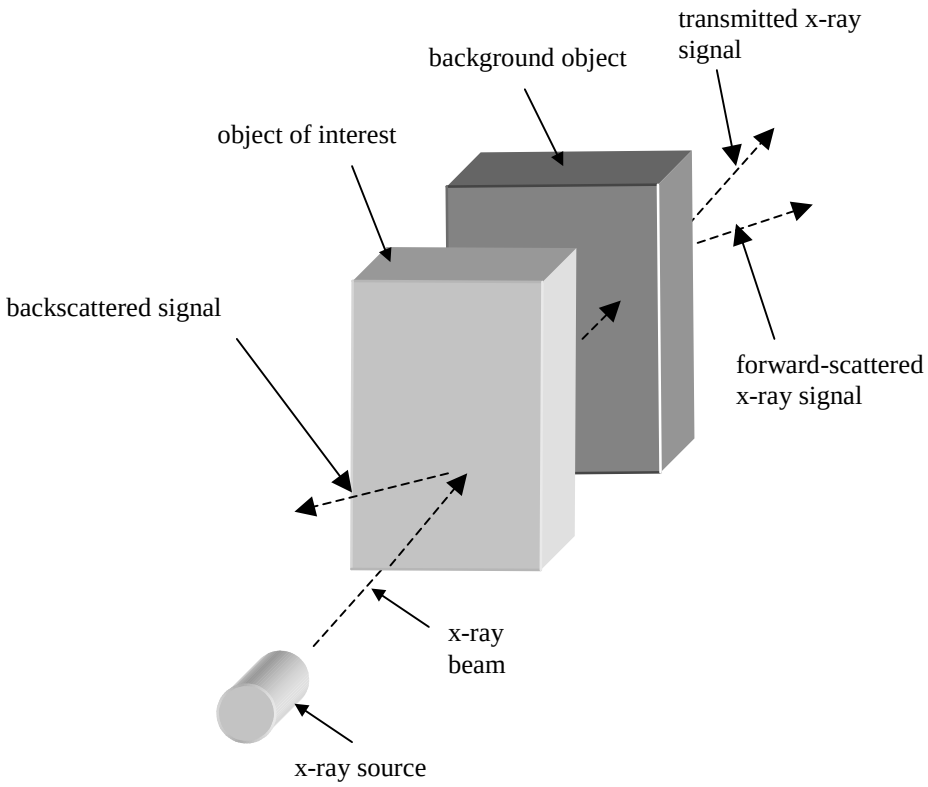

Figure 2.6-1 Illustration of object overlapping.

Being able to obtain the *true* transmission and scatter gray levels of an object of interest is essential for accurate material characterization. The concept is to remove the background overlapping effects and to reveal the *true* gray levels of the object of interest. This problem can only be resolved by using advanced image-processing technology. The purpose of this dissertation is to develop such an image-processing system that is capable of determining an object's *true* gray levels by eliminating its background overlapping effects.

Note that the programming code of the image-processing system developed in this dissertation is system-dependent. More specifically, it is designed for the highly modified AS&E 101ZZ system. However, the methods of removing the background overlapping effects and revealing the *true* gray levels of the object of interest can be applied to many other one-view systems; they are system-independent. This makes this research more meaningful to the explosives detection community.

The image-processing system is quite complex. Each of the following problems must be carefully addressed. They are stated as follows:

Images are collected from four sensing modalities: high-energy transmission, low-energy transmission, forward scatter, and backscatter modalities. Objects in different images must be registered in order to use data from all four sensing modalities. A registration algorithm must be developed for this purpose.

To compute the R and L of an object of interest, this object must also be correctly recognized in a 2-D image. The procedure needed is segmentation. The purpose of segmentation is to decompose an image into different regions where each region has relatively uniform properties, such as gray levels, textures, colors, etc. In an x-ray image, the gray level is usually the property being examined. So an object can be successfully segmented out if it has relatively uniform gray levels across the entire object. Sometimes, boundary information can be useful for splitting and merging two different regions as well. Due to the complexity of x-ray bag images, it is difficult to design an

algorithm that works perfect on every bag image. More likely, the algorithm works well on certain types of images and does not work well on other types of images. However, this segmentation algorithm must be as robust as possible, because it affects not only the recognition of the objects, but also the determination of *true* gray levels of objects. It is possible that an object is segmented into several regions due to the its non-uniformity, and each smaller region has relatively uniform gray levels. But this should not cause any problem because the object shape information is not used in determining its material type, rather the gray levels are.

To eliminate the background overlapping effect, overlapping models must first be created for both transmission and scatter modalities. Mathematical models will be developed for each image modality. Each of these mathematical models contains undefined constants. Then, a number of experiments are performed to obtain the data that can later be used to define values for those constants. The formulation of these models is based on the fact that image gray level is a linear function of x-ray signal intensity.

To eliminate the background overlapping effect, the *true* gray levels of the background overlapped objects must be known. However, from a 2-D image, it is very difficult to find those *true* gray levels because they are completely hidden behind the object of interest. The only possible means is to find neighboring regions that may represent the overlapping background objects, compute the neighboring regions' *true* gray levels, and use this information to eliminate the overlapping effect. An algorithm needs to be constructed to correctly identify the neighboring region representing the background, and to eliminate the background overlapping effect.

This leads to the four things that have been stated in Chapter 1 as objectives for this study. These four things are restated here:

1. Develop an algorithm for spatially registering images collected from the different imaging modalities off the modified AS&E system used in this study.

2. Develop a robust segmentation technique that can identify the entire or parts of objects of interest in the very complex environment presented by passenger luggage.
3. Develop overlapping models so that *true* gray levels of objects can be obtained for transmission and scatter images.
4. Develop an algorithm for determining the *true* gray levels of an object.

Those four things are essential algorithms for improving detection accuracy for a one-view system. Since the system framework has been discussed in Section 1.4, thus no further discussion is given regarding to this aspect of the system.

2.6.2 Overview of the image-processing system

The *R-L* plane based material's characterization requires one to collect four images of a bag: a high-energy transmission image, a low-energy transmission image, a low-energy forward scatter image, and a low-energy backscatter image. These four images are denoted as Img^H, Img^L, Img^F, and Img^B respectively. Img^H and Img^L are needed to estimate the *R* value of an object. Img^L, Img^F, and Img^B are needed to estimate the *L* value of an object. The complete procedure of this image-processing system is explained as follows:

After Img^H, Img^L, Img^F, and Img^B are obtained from the AS&E system, they are preprocessed using the shading correction algorithm to remove non-uniformities in the images. This shading correction algorithm is discussed in Section 3.2. The shading correction algorithm is part of the scanning module. The framework of the entire system is illustrated in Figure 1.4-1.

In order to obtain the *true* gray levels of an object across all four sensing modalities, these four images need to be spatially registered. This registration procedure *registration()* is discussed in Section 4.1. Images are inevitably degraded by noise caused by the x-ray detectors, the x-ray source, and the system's electronic devices. This

noise, if not removed, will significantly affect the computation of *true* gray levels. So images must be filtered to remove at least some part of the noise. This filtering procedure *smoothing()* is discussed in Section 4.2. The *true* gray levels are computed on a region-basis. Each region may represent parts of an object or an object in its entirety. The average gray level is used to represent the *true* gray level of this region in one sensing modality. The purpose of image segmentation is to group image pixels into meaningful regions [JAI95]. Each region has relatively uniform gray levels. The segmentation procedure *segmentation()* is discussed in Section 4.3. All these algorithms are part of the segmentation module.

A footnote regarding the use of the average gray level is that it is not the best representation for a *true* gray level because it cannot represent the gray level variations of a region like a histogram does. However, it is easier to perform arithmetic computation on a mean value. Being able to perform arithmetic computations is important for determining the *true* gray levels of an object. There is no perfect solution to this. Part of the solution is to segment images into regions with relatively uniform gray levels so that mean gray level indeed characterizes this region.

In chapter 5, it is shown that all object overlapping cases can be simplified to a two-object-overlapping case. The models that are used to determine the *true* gray levels of an object of interest when it is overlapped with a background object are developed in Section 5.1. Using those models, procedure *true_gl()* that determines the *true* gray levels of an object of interest in a bag environment is developed in Section 5.2. This algorithm is part of the module for determining an object's *true* gray levels.

The complete procedure *determine_true_gl()* for determining *true* gray levels of objects of interest in a bag can be summarized as follows:

Procedure *determine_true_gl()*

1. Preprocessing Img^L, Img^F, Img^B, and Img^H using shading correction algorithms.

2. Spatially registering Img^F, Img^B, and Img^H to Img^L using procedure *registration()*. After registration, four images are produced Img^H_{Cut}, Img^F_{Cut}, Img^B_{Cut}, and Img^L_{Cut}.
3. Smooth images Img^H_{Cut}, Img^F_{Cut}, Img^B_{Cut}, and Img^L_{Cut} using procedure *smoothing()*. The images after smoothing are Img^H_{Smth}, Img^F_{Smth}, Img^B_{Smth}, and Img^L_{Smth}.
4. Segment image Img^L_{Smth} using procedure *segmentation()*. Two component labeled images are produced: Img^{Lbl}_{Rgn} and Img^{Lbl}_{Obj}.
5. Determine the *true* gray levels of objects of interest using procedure *true_gl()*.

The symbols used throughout this dissertation will follow a set of conventions. The symbol *Img* will always represent an image. The symbol *Rgn* will always denote a region in a segmented labeled image. The symbol *Obj* will always denote an object in an image. The symbol μ will always denote the average gray level of a region. The symbol *I* will always denote the intensity of an x-ray beam. The superscripts that are applied to the above symbols may be *L*, *H*, *F*, or *B*. The superscript *L* indicates that the symbol to which *L* is applied relates to the low-energy transmission modality; the superscript *H* indicates the high-energy transmission modality; the superscript *F* indicates the forward-scatter modality; and the superscript *B* indicates the backscatter modality. The meaning of a symbol including its superscript and subscript will be explained before it is used.

2.6.3 Region-based approach vs. other approaches

Before concluding this section, more discussion will be given as to why a region-based approach is used in developing the image-processing system. There are many different approaches for image-processing algorithm. Existing methods include pixel-based analysis, image decomposition method, histogram characterization methods, and object-based analysis. The image-processing algorithms developed in this dissertation are region-based approach. Different approaches may have different merits and demerits, but

the region-based approach is a better approach for computing *true* gray levels in a bag environment; and it is a better approach for determining the material's types of objects of interest in general.

Pixel-based analysis is developed by Vivid Technologies for dual-energy transmission technology [KRU94, KRU96]. This method has partial capability in removing unwanted background effects to determine the *true* gray level of a pixel. However, since this algorithm does pixel-based analysis, the neighboring pixels of a pixel of interest do not necessarily belong to the background object. The *true* gray level computed for a pixel may not be correct.

Image decomposition method [LEH81] is another method developed by Vivid Technologies. Theoretically, this method can make an accurate detection regardless of the object thickness and the type of object present in the background. But this method can only work for two-object overlapping cases, and often it gives false results if the number of objects overlapped is more than two. In addition, the types of material to be detected must be physically present in a form of filter in the system, and this is sometimes very difficult to attain. The method is designed mostly for operator visualization, and it is not very suitable for automatic computer operation.

The histogram characterization method from AS&E is designed for scatter technology [ANN92]. A histogram from an inspected bag is compared with the histogram from a normal bag. If the histogram of the inspected bag is somehow different from the normal histogram especially in the region of high gray levels, this bag is considered to contain illicit materials [ANN92]. The histogram method uses a statistical analyzing method, an object's information is often entirely ignored; thus false alarms are often made. In addition, the method can not pinpoint the location of the illicit material.

In terms of what should be reported by a detection algorithm, the authorities have set certain guidelines [NAV91]. The detection algorithm should report the following information

- the type of illicit material
- the minimum quantity (mass)
- the object shape (bulk, sheet, thickness, etc.)
- the location of the illicit material in the bag

The image decomposing method and the histogram method cannot report this information. Only the pixel-based method can report this information, though the detection accuracy of this method is relatively low. To overcome the limitations of the pixel-based analysis method, a region-based analysis method is proposed for this study. Each region is formed by pixels with relatively uniform gray levels. Each region may represent an object either partially or in its entirety. It is much easier and more precise to eliminate an object's overlapping effect by finding its overlapping background objects.

A region-based approach is also better than an object-based approach for a number of reasons. First, different objects may appear in a bag in arbitrary orientations and the overlapping situations are complicated; thus it is difficult to identify the boundaries between two different objects. Parts belonging to the same object may have non-uniformed properties such as mass, Z_{eff}, *density*, etc. It is difficult to segment regions on an object basis. Second, if an object is segmented into one region while this object does not have uniform property across the region, and a heuristic value is used to represent this property, it may not reflect the characteristics of each part of the object. Third, though an object-based approach may provide more precise shape information than a region-based approach, many illicit materials, such as plastic explosives and drugs can be molded into any shape; thus the shape information is not very useful for determining an object's material type. For this reason, the author disagrees with other researchers [NAV91] that shape information is required for illicit material detection.

2.7 Chapter Summary

This chapter first gave an overview of the illicit material problem. The illicit material detection problem is clearly defined, and the detection environment is described in detail. There are two major categories of technologies that are used for illicit material detection: bulk technology and vapor technology. In the bulk technology category, x-ray technology is the most promising technology for illicit material detection. X-ray technology relies on determining an object's *density* and Z_{eff} characteristic values to determine the object's material type. Descriptions of x-ray sources and detectors are given. X-ray interaction with matter is also carefully studied. There are many different x-ray technologies. Each x-ray technology is reviewed to show its capabilities in detecting illicit materials. Dual-energy transmission and scatter technologies are described for deriving an object's characteristic values R and L, two values that are related to Z_{eff} and *density*. An object can be tested in the R-L plane to determine its material type. The R and L of an object can only be computed using an object's *true* gray levels. Unfortunately, the *true* gray levels of an object are difficult to obtain due to the fact that an object of interest often overlaps with some background objects in a bag. To resolve this problem, an advanced image-processing system was developed to remove the overlapping effects caused by the background objects and to reveal the *true* gray levels of an object of interest. The remaining chapters in this dissertation will describe the system and the tests that were performed to validate this system's performance.